A Predictive Study of Exotic Higgs Decays for the Run 3 of the ATLAS Experiment

Thesis Submitted in Partial Fulfillment of the Requirements for the Degree of Bachelor of Arts with Honors in Physics.

Author: Jem Guhit
Supervisor: Professor Carlo Dallapicolla
Co-Supervisor: Professor Mark Peterson

Department of Physics
Mount Holyoke College
University of Massachusetts Amherst

Acknowledgements

I would first like to thank my thesis advisor, Professor Carlo Dallapiccola of University of Massachusetts Amherst. Professor Dallapiccola's office was always open whenever I ran into difficulties, had a question about my research, and writing. He consistently allowed this paper to be my own work, and guided me in the right the direction whenever he thought I needed it.

I would also like to thank the Professors who were involved in the completion of this research project: Professor Mark Peterson and Professor Kerstin Nordstrom of Mount Holyoke College. To Professor Peterson, my thesis advisor liaison, I would like to thank you for your help in proofreading the thesis paper, providing insightful advice, and stimulating my critical thinking. To Professor Nordstrom, my academic advisor, thank you very much for always having my back and for supporting my endeavors.

I would also like to acknowledge the Physics Department of Mount Holyoke College for their unending support during my undergraduate years.

Finally, I would like to give thanks to my family, parents, and sister for providing me with unfailing support and continuous encouragement throughout my years of study and through the process of researching and writing this thesis. This accomplishment would not have been possible without them. Thank you.

Abstract

The Large Hadron Collider (LHC) in Geneva, Switzerland has made an astounding discovery in 2012 when it detected a particle mimicking the properties of the Higgs Boson which causes spontaneous electroweak symmetry breaking which gives masses of current known particles. However, the true structure and dynamics of this scalar boson is still unknown. One of the theories suggest the involvement of the newly discovered boson particle in the dark matter sector, which hypothesizes that an analog dark Higgs mechanism breaks the $U(1)_D$ dark gauge symmetry. The theory lays the foundation of possible theoretical decay channels of a Higgs Boson to decay to dark charge particles in the dark matter sector that is mediated by a vector boson called the dark photon, Z_D. The upcoming High Luminosity-LHC (HL-LHC) would significantly extend the sensitivity of these direct searches. This thesis focuses on a predictive study of the exotic higgs decay mode, H $\rightarrow Z_D Z_D \rightarrow$ 4l for the run 3 of the ATLAS Experiment in the LHC. Using Monte Carlo (MC) simulated data sets of dark photon mass ranges, $20 < Z_D < 60$ GeV for the signal data and the previous run 2 data set for the background data, the efficiency is calculated to solve for the cross section of the signal. Using the built-in statistical methods in ROOT, the 95% Confidence Level (CL) Upper-Limit (UL) of the signal would be calculated and then be converted to a 95% CL UL Cross-Section ($\sigma^{95\%CL,UL}$) for run 3.

Introduction

In 1964, Peter Higgs together with Francois Englert developed a theory that explains the origin of mass of elementary particles. The theory, most commonly known as the Higgs Mechanism, predicted the existence of a scalar particle. In the summer of 2012, the ATLAS and CMS Collaborations at the LHC discovered a particle at a mass of 125 GeV consistent with the predictions of the Brout-Englert-Higgs (BEH) Mechanism. The scalar particle, most famously known as the Higgs Boson opened up a completely new field of study that has the potential to improve our current knowledge of the Standard Model and the opportunity of exploring the kinematics of the Higgs Boson.

Since the Higgs Boson is still considered a recently discovered particle, there are unanswered questions about its type, states, and decay modes. There are ongoing studies that aim to determine all possible decay modes of the Higgs Boson, and one of these studies is based on the theory that links the Higgs Boson to decay to beyond the standard model (BSM) particles. The research group is focused on the theory that predicts an analogous $U(1)$ symmetry group in the dark sector that leads to the appearance of the BSM vector boson known as the dark photon, Z_D.

Utilizing the datasets from the previous run of the LHC at 7 and 8 TeV, physicists saw the possibilities of the Higgs Boson decaying to exotic particle states where "exotic" characterizes a type of decay that violate known laws of physics and involve new light states beyond the SM. In order to gain evidence of an observation or even discovery of exotic Higgs decays, the current capabilities of the LHC are not sensitive enough to probe the sector. Plans have been made to increase the luminosity of the LHC and hardware upgrades of the detector to improve the physics capacities of the collider. In line with the upgrades, this thesis is a predictive study of a specific exotic higgs decay, $H \rightarrow Z_D Z_D \rightarrow 4l$, for the run 3 of the ATLAS experiment at the LHC in CERN with an integrated luminosity of $\mathcal{L}_{int} = 300\ fb^{-1}$. The discovery of the dark photon and evidence for this process could lead to a significant advancement in our understanding of the physical world and would bridge the gap between the Standard Model and dark matter sector.

This study is based on MC Simulated datasets of the signal events and using the previous run 2 data for the background events. Another important component of this study are the algorithms used to extract the signal efficiency and

upper limit of observed events at 95% CL. Using these components along with the extrapolated background signal for run 3, the upper limit cross section at 95% confidence level can be calculated. Lower values of the upper limit cross sections are considered progress for the study because it improves the precision of the possible kinematics of the decay mode.

This thesis begins with a general introduction into the theoretical basics in Chapter 1. Chapter 2 discusses the discovered scalar particle in detail. Chapter 3 deals with the BSM theories relates Higgs decaying to exotic particle states. Chapter 4 talks about the important components of the ATLAS detector. In Chapter 5, the selection of data and simulated samples are discussed followed by the analysis in Chapter 6. Chapter 7 contains the application and the results of the analysis of the Monte Carlo samples and presents future work and direction for the project.

Contents

1 Introduction to the Standard Model **1**
1.1 Overview of Particles . . . 1
1.1.1 Leptons . . . 2
1.1.2 Quarks . . . 4
1.1.3 Gauge Bosons . . . 5
1.2 Fundamental Interactions . . . 6
1.2.1 Electromagnetic Interaction . . . 7
1.2.2 Weak Interaction . . . 9
1.2.3 Strong Interaction . . . 10

2 The Higgs Boson **13**
2.1 Spontaneous Electroweak Symmetry Breaking . . . 13
2.2 Role of the Higgs Boson . . . 14

3 Physics Beyond the Standard Model **19**
3.1 Motivation of Exotic Higgs Decays . . . 19
3.2 SM + Vector . . . 20
3.3 $\mathbf{H \to Z_D Z_D \to 4l}$ . . . 20

4 ATLAS Experiment **23**
4.1 The ATLAS Detector . . . 24
4.1.1 Inner Detector . . . 25
4.1.2 Calorimeter . . . 27
4.1.3 Muon Spectrometer . . . 28
4.1.4 Magnet System . . . 29
4.2 Trigger System . . . 30

5 Data, Simulated Samples, and Event Selection **31**
5.1 Signal and Background Sample Data . . . 31
5.2 Event Selection Criteria . . . 32
5.2.1 Trigger Requirements . . . 32
5.3 BSM Signal Samples . . . 33
5.3.1 Previous ATLAS Paper . . . 33
5.3.2 Current Study . . . 34
5.4 SM Background Samples . . . 34
5.4.1 Previous ATLAS Paper . . . 34
5.4.2 Current Study . . . 34

6 Data Analysis **35**
6.1 Scaling of Background 36
6.1.1 Uncertainties 36
6.2 Efficiency (ϵ_S) 37
6.3 Upper Limit of Signal (N_S^{obs}) 40
6.3.1 Poisson Processes 40
6.3.2 Hypothesis Testing 40
6.3.3 Confidence Intervals and Upper Limits 41
6.3.4 Method of Calculating N_S^{obs} 41
6.4 Upper Limit of Cross Section ($\sigma^{95\%CL,UL}$) for Run 3 42
6.4.1 Derivation of Cross Section Equation 42
6.4.2 Calculating for $\sigma^{95\%CL,UL}$ 43
6.5 Upper Limit of Cross Section ($\sigma^{95\%CL,UL}$) for Run 2 44

7 Results for the Data Samples **46**

8 Summary and Next Steps **48**

A Appendix **49**

Bibliography **71**

List of Figures

1 Elementary particles included in the Standard Model [41] 2
2 $e^-e^- \to e^-e^-$ 8
3 Fermi's Original Fermion Four Point Interaction 9
4 $p + n \to e + \bar{v}$ 10
5 Diagram showing the concept of color charge within quarks and anti-quarks [32][31] 11
6 Possible Feynman Diagrams for Strong Interaction: gluon-gluon coupling and quark-gluon coupling 12
7 Plots showing the observation of a new particle at 5σ [25] 17
8 Decay Modes Under SM + V Theory [33]. Region A is the region where $h \to Z_D Z_D$ is the dominant decay, where the red dotted line is when $m_s = m_h$. Region B shows when the following decays occur: $h \to ss$ and $h \to Z_D Z_D$ (Theory not considered in this thesis), Region C has no predicted decays, and Region D shows that the decay $h \to ss$ occurs (Theory also not considered in this thesis). The black contours is the parameter $\kappa \times 10^3$ required for the $\mathrm{Br}(h \to Z_D Z_D, ss) = 10\%$ 21
9 Dominant Exotic Higgs Decay under Kinetic Mixing [37] 22
10 One Type of Exotic Higgs Decay under Higgs Mixing [37] 22
11 One Type of Higgs Decay under Higgs Mixing [33] 22
12 Major LHC Experiments [22] 23
13 ATLAS Detector [24] 24
14 Inner detector showing the pixel detector, semiconductor trackers, and transition radiation trackers [91] 25
15 Electromagnetic and Hadronic Calorimeters along with other components [91] 27
16 Muon Spectrometer components [91] 28
17 Magnet System [26] 29
18 Illustration of Background and Signal Data 31
19 Diagram illustrating a brief overview of the data analysis method 35
20 Residuals at $m_{Z_D} = 20$ GeV and $c\tau = 50$ cm where $S_f = 29139$ events 38
21 Residuals at $m_{Z_D} = 40$ GeV and $c\tau = 50$ cm where $S_f = 6728$ events 38
22 Residuals at $m_{Z_D} = 40$ GeV and $c\tau = 500$ cm where $S_f = 2483$ events 38

23 Residuals at $m_{Z_D} = 60$ GeV and $c\tau = 50$ cm where $S_f = 7999$ events 39
24 Residuals at $m_{Z_D} = 60$ GeV and $c\tau = 500$ cm where $S_f = 3361$ events 39
25 95% CL UL $(\sigma \times B)$ (pb) vs. range of $c\tau$ (cm) for $m_{Z_D} = 20$ GeV [28] 44
26 95% CL UL $(\sigma \times B)$ (pb) vs. range of $c\tau$ (cm) for $m_{Z_D} = 40$ GeV [28] 45
27 95% CL UL $(\sigma \times B)$ (pb) vs. range of $c\tau$ (cm) for $m_{Z_D} = 60$ GeV [28] 45
28 Illustration of a smaller $\sigma^{95\%,UL} \times B$ 46

List of Tables

1 Summary of Interactions, Force Carriers, and Underlying Theories [49] 6
2 MC signal samples for the dark-sector model. For all samples, $m_H = 125$ GeV, $\sigma(pp \to H) = 44.1$ pb and $\text{Br}(H \to Z_D Z_D) = 0.10$ [29] 33
3 Efficiency values for MC simulated signal datasets 40
4 95% CL Upper-Limit of the signal with Optimistic Background event of 127 ± 11 events with $N_S^{obs} = 32.815$ events 42
5 95% CL Upper-Limit of the signal with Pessimistic Background event of 127 ± 45 events with $N_S^{obs} = 117.877$ events 42
6 $\sigma^{95\%CL,UL} \times B$ with Optimistic Background event of 127 ± 11 events 43
7 $\sigma^{95\%CL,UL} \times B$ with Pessimistic Background event of 127 ± 45 events 44
8 The 95% CL Upper-Limit $\sigma\times$ B for run 2 ($\sigma_{R2}^{UL} \times B$), the optimistic 95% CL Upper-Limit $\sigma\times$ B ($\sigma_{R3.1}^{UL} \times B$), and the pessimistic 95% CL Upper-Limit $\sigma\times$ B ($\sigma_{R3.2}^{UL} \times B$) for run 3 in fb for the various masses of the Z_D in GeV and their respective lifetime, $c\tau$, in cm . 46

1 Introduction to the Standard Model

In our modern world, we understand matter and energy through the kinematics and interaction of elementary particles. Through the years, scientists have studied physics laws with the aim of reducing them to a set of fundamental theories. One of the unifying the laws of theories which attempt to explain all the phenomena of particle physics in terms of the properties and interaction of particles is called the Standard Model (SM) [73]. The theory has demonstrated years of huge successes in making experimental predictions. However, the Standard Model is incomplete because it does not give an accurate model for gravitation and does not fully explain some properties of the elementary particles [21] . The gaps in the Standard Model leave extensive areas for scientists to study theories extending to dark matter and discover new physics Beyond the Standard Model (BSM).

At present, matter is believe to be made out of three elementary particles: leptons, quarks, and gauge bosons. The four fundamental forces are electromagnetic interaction, weak interaction, strong interaction, and gravitation. The electromagnetic interaction is the force that acts between charged particles. The weak interaction is the force that acts between subatomic particles causing radioactive decays. The strong interaction holds ordinary matter by binding quarks into hadrons such as protons and neutrons in order to create atomic nuclei. Gravitation is the weakest force of all the interaction and remains unexplained in terms of the SM [99]. This chapter discusses a phenomenological overview of elementary particles and their fundamental interactions.

1.1 Overview of Particles

There are two main classifications of particles: fermions and bosons. Fermions are non-integer $spin - \frac{1}{2}$ particles that obey Pauli's exclusion principle, which states that two particles cannot occupy the same quantum state at any given time [79]. In the Standard Model, there are 12 fermions categorized as leptons and quarks with each particle having a corresponding antiparticle. There are six quarks (up, down, charm, strange, top, bottom), and six leptons (electron, electron neutrino, muon, muon neutrino, tau, tau neutrino).

Unlike fermions, bosons do not obey Pauli's exclusion principle and do not have restrictions on the number of identical particles that occupy the same quantum state [78]. The integer spin particles are made out of both elementary and composite particles. In the Standard Model, there are five elementary bosons: photon, gluon, Z neutral weak boson, $W^{\pm}$ charged weak bosons, and the Higgs Boson.

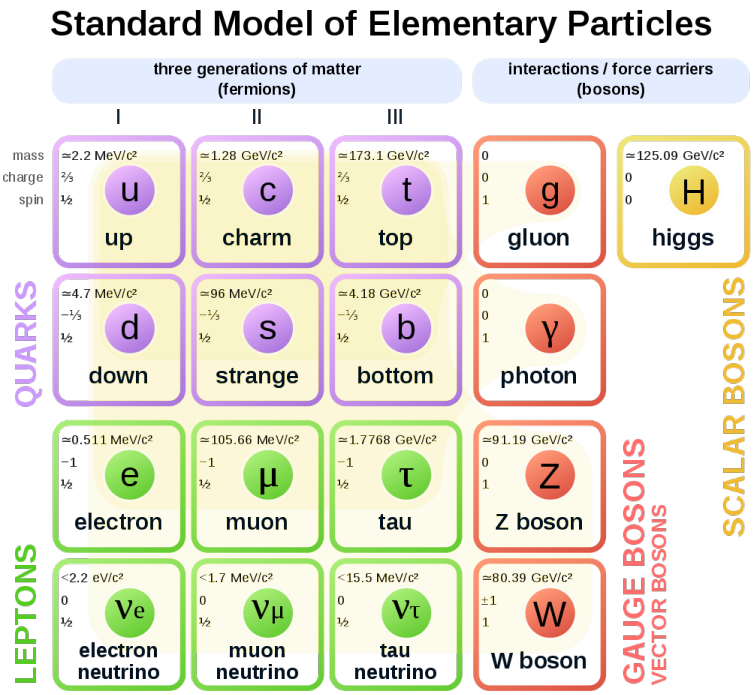

Figure 1: Elementary particles included in the Standard Model [41]

The first four bosons are force carriers of fundamental interactions and are called Gauge Bosons.

1.1.1 Leptons

Leptons are one of the three classes of fundamental particles in the standard model. The six types of leptonic particles, known as "flavours", are classified into three generations. The first is comprised of the electron (e^-) and electron neutrino (ν_e), the second generation with the muon (μ^-) and muon neutrino (ν_μ), and the third generation with the tauon (τ^-) and tauon neutrino (ν_τ) with each generation having a heavier mass than the previous [68]. The generation of leptons are written as doublets in (1). Each lepton is associated with its own antiparticle denoted by (e^+, μ^+, τ^+) and ($\bar{\nu_e}$, $\bar{\nu_\mu}$, $\bar{\nu_\tau}$) The section discusses the following intrinsic properties of leptons: Spin, Electromagnetic Interaction, Weak Interaction, and Lepton Numbers.

$$\begin{pmatrix} e^- \\ \nu_e \end{pmatrix}, \begin{pmatrix} \mu^- \\ \nu_\mu \end{pmatrix}, \begin{pmatrix} \tau^- \\ \nu_\tau \end{pmatrix} \tag{1}$$

Spin: Leptons are one type of fermions and are $spin - \frac{1}{2}$ particles.

Electromagnetic Interaction: An important property of leptons is their electric charge, Q. It determines the strength of the electric field the particle

generates and its effect on the other particles. A generation contains a charged lepton with Q = -e, and another lepton with Q = 0. Hence, leptons are also categorized as *charged leptons (e^-, μ^-, and τ^-) neutral leptons (ν_e, ν_μ, and ν_τ)* [68].

Weak Interaction: The weak force is responsible for lepton change flavours (e.g e^- to ν_e) through force carriers [81].

Lepton Number: Conservation laws were developed to determine which reactions are permitted and forbidden. Each generation's doublet is assigned leptonic numbers that are conserved under the Standard Model. All leptons in each generation have L = 1, while the antileptons have L = -1 [50].

Brief History

The first lepton discovered was the electron in an experiment led by J.J Thomson in 1897 [95], while Wolfgang Pauli discovered the electron neutrino in 1930 to understand the phenomena of β decays [68]. Pauli hypothesized that the neutral particle electron neutrino preserved the conservation of energy and momentum in the decays.

In 1936, Carl Anderson and Seth Neddermeyer discovered the second generation lepton, the muon. The particle's discovery is credited to Anderson and Neddermeyer's study of high energy Cosmic ray particle collisions in the earth's atmosphere [69]. The newly discovered particle had similar properties to the electrons and only differed in mass. Meanwhile in 1962, Leon Lederman, Melvin Schwartz, and Jack Steinberger completed the second generation doublet pair by first detecting interactions of the muon neutrino through an experiment at Brookhaven National Laboratory, which earned them the 1988 Nobel Prize [38].

The tauon was discovered in 1975 by a collaboration of Martin Lewis Perl and Yung-Su Tsai through electron–positron annihilation experiments at high energies in Stanford Linear Accelerator Center (SLAC) and Lawrence Berkeley National Laboratory (LBL) group [84]. Further studies confirmed the tauon to be a point-like $spin - \frac{1}{2}$ particle with similar electromagnetic interaction properties as the electron and muon making it the third generation lepton. Due to electron and muon having corresponding neutrinos, it was also expected for the tau to have an associated neutrino. The DONUT Collaboration in Fermilab detected the tau neutrino in 2000, making it the most recent particle to be discovered before the Higgs Boson in 2012 [62].

1.1.2 Quarks

The Quark Model, originally developed by Murray Gell-Mann and George Zweig in 1964, is also one of the three classes of fundamental particles in the standard model [17] . Similar to leptons, there are six distinct types or "flavours" which occurs in pairs or three generations. The first is comprised of the up and down quark, the second generation with charm and strange quark, and the third generation with the top and bottom quarks with each generation also having a heavier mass [72]. The generations of quarks are written as doublets in (2). Each quark is associated with its own antiparticle denoted by ($\bar{u}$,$\bar{c}$,$\bar{t}$) and ($\bar{d}$,$\bar{s}$,$\bar{b}$). This section discusses the following intrinsic properties of quarks: Spin, Electric Charge, Weak Interaction, Strong Interaction and Colour, and Baryon Number.

$$\begin{pmatrix} u \\ d \end{pmatrix}, \begin{pmatrix} c \\ s \end{pmatrix}, \begin{pmatrix} t \\ b \end{pmatrix} \tag{2}$$

Spin: Quarks are one type of fermion and are $spin - \frac{1}{2}$ particles.

Electric Charge: In each generation, one quark contains a charge of $+\frac{2}{3}$ (u, c, and t) and the other quark of the pair contains a charge of -$\frac{1}{3}$ (d, s, and b) [72]. Similar to leptons, each quark is associated with its own antiquark with charges opposite to their counterpart particle. Quarks make up composite particles called hadrons which have two types: baryons and mesons. Baryons are composed of a combination of three quarks while Mesons contain a quark and an antiquark pair [72]. Summing the charges of the constituent quarks, all hadron particles have integer charges. For example,

$$\text{Hadron: Proton (uud)} = \tfrac{2}{3} + \tfrac{2}{3} - \tfrac{1}{3} = +1\text{e}.$$

$$\text{Meson: Pion } (u\bar{d}) = \tfrac{2}{3} + \tfrac{1}{3} = +1\text{e}$$

Weak Interaction: Similar to leptons, the weak force is responsible for quark changing flavours through force carriers. Any up-type quark (u, c, and t) can change into any down-type quark (d, s, and b) and vice versa [72].

Strong Interaction: According to quantum chromodynamics (QCD), a topic in quantum field theory, quarks possess a property called color charge [80]. There are three types of color charge: blue, green, and red, where each is complemented by an anticolor – antiblue, antigreen, and antired . Every quark carries a color, while every antiquark carries an anticolor.

Baryon Number: Similar to leptons, quarks and hadrons are assigned baryon numbers that are conserved under the Standard Model. All baryons in each generation have B = 1, while the antibaryons have B = -1 [50].

Brief History

The beginnings of the quark model occurred in 1947, where new types of hadrons were discovered in cosmic rays experiments from research groups in Universities of Bristol and Manchester [72]. As intense beams of particles at higher energies became more available at accelerator laboratories, scientists continued to discover more hadrons that needed further explanation using a theoretical framework. In 1964, Murray Gell-Mann and George Zweig proposed the quark model, where they postulated that hadrons could be interpreted as bound states of fundamental $spin - \frac{1}{2}$ particles together with their antiparticles [18]. They proposed that all baryons were composed of triplets of quarks (selected from u, d and s) and the mesons were doublets formed by a quark and an antiquark. The three quark model was extensively used in the 1960's and was further confirmed by experiments from the Stanford Linear Accelerator (SLAC) in Stanford, California during the early 1970's.

The Quark Model continued to expand when Sheldon Glashow, John Iliopoulis, and Luciano Maiani predicted the existence of the fourth quark called the Charm quark [87]. The particle was officially detected in 1974 in experiments from SLAC and Brookhaven National Laboratory (BNL) by discovering the particle J/ψ which decays to a charm and anti-charm quark [19]. The new quark was more massive than the proton at 1,200 MeV and had a charge of $\frac{2}{3}$e like the up quark [87]. With the pairs (e^-, ν_e) and (μ, ν_μ), a symmetry was established between quarks and leptons but was disrupted with the discovery of the fifth quark. In 1977, Leon Lederman's group at Fermilab discovered an upsilon meson, Υ, and detected that it decays to a bottom and anti-bottom quark pair [87]. Ever since the discovery of the bottom quark, scientists have been anticipating of detecting its pair, the top quark to maintain the symmetry. Collecting enough evidence from the CDF and $D\phi$ collaborations, the two groups jointly reported the discovery of the top quark in March 1995 with a mass of approximately 176 GeV [20].

1.1.3 Gauge Bosons

Gauge Bosons are bosonic particles that carry any of the fundamental interactions of nature. All known gauge bosons are spin-1 particles and are classified as vector bosons [73]. The Standard Model of particle physics currently recognizes four kinds of gauge bosons: photons, which carry the electromagnetic interaction; W and Z bosons, which carry the weak interaction; and gluons, which carry the strong interaction [49]. The fundamental interactions and their underlying theories would be discussed in more detail later in the chapter.

Photon: Photons are elementary particles travelling at the speed of light and exhibiting properties of waves and particles [73]. The photon is massless, has no electric charge, and is a stable particle. Furthermore, since it is electrically neutral, the photon is its own antiparticle. The electromagnetic force is mediated by this massless particle by coupling to charged particles. Hence, only charged particles interact via the electromagnetic force.

$W^{\pm}$ and Z Bosons: The $W^{\pm}$ and Z Bosons are force carriers of the weak force and are more massive particles [51]. First studies and discovery of the W and Z boson were done through the UA1 and UA2 Experiments at the Super Proton Synchrotron (SPS) collider in CERN in 1983 (CERN). The absorption and emission of a $W^{\pm}$ can raise or lower an electric charge and alter the spin of the particle. Also, the absorption and emission of a W boson can change the type of the particle. On the other hand, the neutral Z boson cannot change the electric charge of a particle [69].

Gluons: Gluons are force carriers for the strong force between quarks [80]. These bosons "glue" quarks together, which in turn form hadrons such as protons and neutrons. A special feature of this vector boson is that they carry the "color" charge of the strong interaction [54]. Therefore, unlike a photon that doesn't have a charge, gluons both participate and mediate in the strong interaction making them harder to study compared to other interactions.

Force	**Strength**	**Range**	**Theory**	**Mediator**
Strong	10	10^{-15}	Chromodynamics	Gluon
Electromagnetic	10^{-2}	Infinite	Electrodynamics	Photon
Weak	10^{-13}	10^{-15}	Flavordynamics	$W^{\pm}$ and Z
Gravitational	10^{-42}	Infinite	Geometrodynamics	Graviton

Table 1: Summary of Interactions, Force Carriers, and Underlying Theories [49]

1.2 Fundamental Interactions

Quantum Mechanics describes the microscopic nature of atoms and subatomic particles. Physicists extensively studied the implications of Schrodinger's equation, which describes the non-relativistic version of quantum mechanics [14]. Since Particle Physics is a study that combines quantum mechanics and special relativity, the relativistic version of quantum mechanics called Quantum Field Theory (QFT) was developed to explain how forces work. There are currently four known fundamental forces. The electromagnetic force is described by Quantum Electro-

dynamics (QED), the strong nuclear force is described by Quantum Chromodynamics (QCD), the weak nuclear force is described by the Electroweak theory (EWT), and the force of gravity is not yet fully explained by the standard model. All the processes that occur through different fundamental interactions within the Standard Model are described by Feynman Diagrams [58]. Developed by Richard Feynman in 1948, the diagrams give a simple visualization of the mathematical calculations.

Introduction to Gauge Theory

Gauge Theory is a Quantum Field theory developed to mathematically describe the Standard Model and explain known fundamental interactions. These fields, however, cannot be directly measured and associated quantities such as charges, energies, and velocities can be measured to study properties and determine the different types of fields [83]. There is possibility that different configurations of non-observable fields can result in identical observable quantities. A transformation from one such field configuration to another is called a *gauge transformation*, while if measurable quantities are invariant despite the transformation is a property called *gauge invariance*. Since invariance under a field transformation is considered a symmetry, then gauge invariance is also called *gauge symmetry* [83]. Therefore, any theory that has the property of gauge invariance is considered a gauge theory.

The Standard Model is explained by a gauge quantum field theory containing the internal symmetries of the unitary product group $U(1) \times SU(2) \times SU(3)$ with its interactions mediated by particles called gauge bosons.

1.2.1 Electromagnetic Interaction

The electromagnetic force is described by Quantum Electrodynamics (QED) and mathematically explained by an abelian gauge theory based on a symmetry group called U(1) [13]. As one of the first quantum field theories to be discovered, in 1927, Paul Dirac developed the first quantum theory of the electromagnetic field that explains the decay of an atom to a lower state and how it follows energy conservation laws [67]. Physicists helped extend Dirac's idea to form the basis for modern QED theory, which treats photons as a particle that mediate the electromagnetic force. All charged particles interact via the electromagnetic force by emitting and absorbing photons [49]. Since photons are mass-less and travel at the speed of light, they do not interact with each other. The effects of electromagnetism are produced from the energy and momentum the photon carries

when it gets emitted or absorbed by a particle [92].

The photons that mediate the electromagnetic interaction are known as virtual particles [49]. In a particle process, there exists an initial and final state which follows the conservation laws. The virtual particles are created when a particle emits or absorbs a photon. The range of fundamental forces can be explained through Heisenberg's Uncertainty Principle, which has a position-momentum and energy-time version [15]. To determine the particle lifetimes, we use the energy-time equivalent.

$$\Delta E \Delta t \approx \frac{\hbar}{2} \tag{3}$$

From quantum field theory, an interaction between two particles, A and B, occurs with the exchange of a gauge boson, X. A emits X with a mass of m_X which travels and is absorbed by B. The lifetime of the gauge boson is t_X, given by the distance it travels as $d \approx ct_X$. From equation (3), Δt is defined as the lifetime of X and ΔE as the rest mass of the X where,

$$\Delta E = m_x c^2 \tag{4}$$

Substituting equation (4) to (3) we have,

$$\Delta t m_x c^2 \approx \frac{\hbar}{2} \tag{5}$$

$$\Delta t \approx \frac{\hbar}{2 m_x c^2} \tag{6}$$

Finally, substituting $\Delta t = \frac{d}{c}$ to equation (6), the range of the gauge boson is defined as:

$$d \approx \frac{\hbar}{2 m_x c} \tag{7}$$

Since the photon is massless ($m_x = 0$), then the virtual photon's range is infinite making the electromagnetic interaction a long-range force.

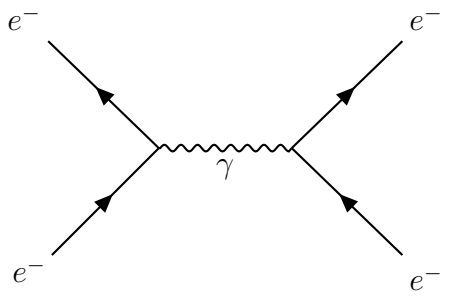

Figure 2: $e^-e^- \rightarrow e^-e^-$

In the Feynman diagram in Figure 2, two electrons enter and the point where the lines connect to other lines is a vertex. This is where the particles meet and interact, by emitting or absorbing particles. In the electromagnetic interaction, the process is mediated by the photon then the two electrons exit [49]. The diagram describes the interaction between two electrons and shows a photon emitted at the first vertex and absorbed at the second vertex. Furthermore, we could also deduce from the diagram the strength of the electromagnetic interaction denoted by the coupling constant, α [79]. The coupling constant is proportional to the square of the unit charge (e), which appears for each vertex in the diagram [49]. For this specific example there are two vertices therefore $\alpha = e^2 \approx \frac{1}{137}$.

1.2.2 Weak Interaction

The weak nuclear force is described by the Electroweak Theory (EWT) and mathematically explained by a non-abelian gauge theory based on a symmetry group called $U(1) \times SU(2)$ [13]. The development of weak interactions started with Henri Becquerel's discovery of radioactivity in 1896, which enabled other scientists such as Rutherford to classify three distinct radioactive decays: alpha, beta, and gamma [89]. In 1933, Enrico Fermi developed a mechanism for the process which improved the understanding of beta decays [98]. Fermi incorporated Pauli's postulate about a massless neutral particle, called a neutrino, being emitted (Rajasekaran, 2014, p. 2). Since in electromagnetic interactions, a photon is emitted and absorbed by a lepton at a quantum level, Fermi made an analog in weak interactions in a beta decay where an electron-neutrino pair is emitted. The strength of the weak interaction is determined by the Fermi Coupling constant at $G_F = \frac{10^{-5}}{m_p^2}$, where m_p is the proton mass [89].

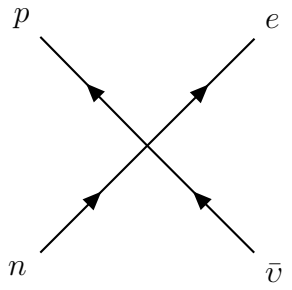

Figure 3: Fermi's Original Fermion Four Point Interaction

Applying Fermi's theory of weak interactions to beta decay, he initially thought that the neutron - proton line and electron-neutrino line interacted at the same space time point coining the term fermion four-point interaction [90]. However, through years of research and validation from experiments, Fermi's Weak Interaction transitioned to the current version called Electroweak Theory. In Fermi's

Weak Interaction Theory, he postulated that the coupling constant was G_F. The difference is that the two pairs of lines are separated by an exchange of a certain boson called W. Hence, in the Electroweak Theory there is a coupling constant g at each vertex. In the same beta-decay process, two vertices mean a factor of g^2. Therefore, the strength of the weak interaction is determined by the Fermi Coupling constant at $G_F = \frac{\sqrt{2}g^2}{8m_W^2}$ where m_W is the mass of the boson that mediated the process [90].

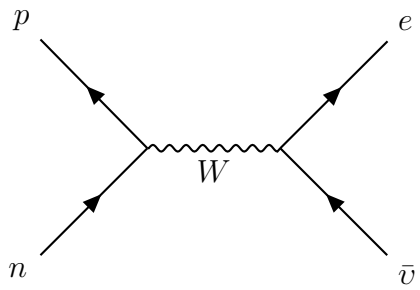

Figure 4: $p + n \rightarrow e + \bar{v}$

For a general gauge group, the number of force-carriers is always equal to the dimension of the adjoint representation. For the simple case of SU(N), the dimension of this representation is N^2-1 [66]. The dimensions of the SU(N) group explains that for the weak interaction there are $2^2 - 1 = 3$ gauge bosons. Upon the discovery of the $W^{\pm}$ and Z bosons, in contrast to photons, these gauge bosons are massive. Using equation (7), it can be deduced that the weak interaction is a short-range force. Therefore, Fermi's coupling constant has taken the shape into its current form, $G_F = \frac{\sqrt{2}e^2}{8sin^2\theta_W m_W^2}$ where θ_W, also called the *weak mixing angle* is an important parameter of the electroweak theory and has been determined experimentally, $sin\theta_W = 0.23$ [90].

1.2.3 Strong Interaction

The strong force which is described by Quantum Chromodynamics (QCD) and mathematically explained by a non-abelian gauge theory based on a symmetry group called SU(3) [13]. The foundations of the strong nuclear force started with developments in Nuclear Physics regarding the atom and its nucleus. Scientists initially thought that the nucleus contains electrons, which keeps the nucleus together. In 1911, Ernest Rutherford discovered the presence of protons in the nucleus [53]. The discovery rejected the postulate that electromagnetic force is responsible for holding particles within the nucleus of the atom because it would cause further repulsion to the positive charge of the protons. Upon James Chadwick's discovery of the presence of neutrons in the nucleus in 1932, Eugene Wigner suggested that the electromagnetic force is not responsible for holding

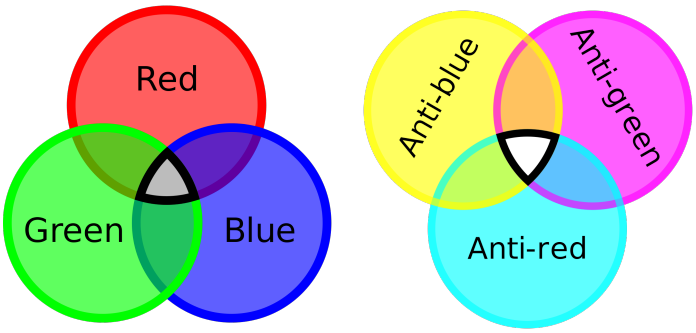

Figure 5: Diagram showing the concept of color charge within quarks and anti-quarks [32][31]

the particles together in the nucleus and that the phenomena involved another type of nuclear force [64]. The strong nuclear force is the nuclear binding force the that provides the attraction between protons and protons, proton and neutrons, and neutrons and neutrons, which keeps the nucleus of atoms together [51].

In the strong interaction, the gauge boson mediating the process is the gluon. Since gluons are massless it would be immediately thought that from equation (7), the strong force would be a long-range force as well. However, the two forces are different, as the strong force possesses another feature called *color charge* [71]. Figure 5 shows the color charge scheme for quarks and anti-quarks and it is a property related to the particles' strong interactions (QCD). The color charge of quarks and gluons is unrelated to the real meaning of color and makes use of the idea that mixing primary and complementary colors results in a white or colorless color (Nave). Quarks contain the the primary colors red, blue, and green while anti-quarks contain the secondary colors yellow, magenta, and cyan. When all the three colors and anti-colors are mixed together, the result is "colorless" or "white" which translates to the strong interaction having a net color charge of zero (Martin, 2008, p. 163). The hadrons have a color charge of zero, with baryons composed of three quarks and mesons composed of a quark and anti-quark pair. Gluons also possess a color charge, and based on the dimensions of a simple SU(N) group, there are $3^2 - 1 = 8$ gluons possessing color charge to maintain conservation of color charge.

In the electromagnetic interaction, the photon does not interact with the particles because it does not have an electric charge. But in the strong interaction gluons carry color charge, which allows them to participate in both gluon-gluon and quark-gluon processes. Furthermore, another major difference between QED and QCD are their coupling constants. From section 1.2.1, the electromagnetic interaction has a coupling constant of $\alpha = \frac{1}{137}$, which suggests a perturbation the-

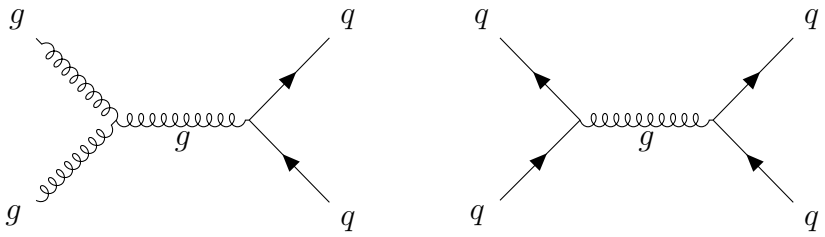

Figure 6: Possible Feynman Diagrams for Strong Interaction: gluon-gluon coupling and quark-gluon coupling

ory expansion [49]. For the strong interaction, this is not the case. The coupling constant,α_s ,was determined experimentally to be greater than 1. It was later discovered that α_s was rather a *running coupling constant*, which depended on the separation distance of interacting particles [49]. At large distances, $\alpha_s >> 1$ which implies that the particles cannot be isolated. The α_s increases at low energies and the phenomenon is called *Color Confinment*. On the other hand, at shorter distances, $\alpha_s << 1$ which implies that the particle's coupling strength decreases which allows perturbative calculations. The α_s decreases at high energies and this phenomenon is known as *asymptotic freedom* [70]. The running coupling constant, and behavior of particles at high and low energies explains why the strong interaction is a short-range force.

2 The Higgs Boson

From Chapter 1, physicists were able to determine a unified relationship between the weak and the electromagnetic force. The fundamental symmetry between the forces established that eletromagnetism and radioactivity are phenomenon that occur through the **Electroweak Force**. However, distinct differences between the interactions and gauge bosons mediating the forces raised questions on the validity of the unified theory. As recalled from the previous chapter, the Standard Model is a Gauge Theory whose main properties are symmetry and invariance. The weak interactions are short-range which meant that the $W^{\pm}$ and Z bosons that mediate interaction are massive while the photon that mediates the long-range electromagnetic force, is massless. The differences between the electromagnetic and weak interaction have sparked debates and raised an issue on its unification.

This chapter gives an overview of the spontaneous symmetry breaking of the Electroweak theory, a brief introduction to a fourth gauge boson known today as the *Higgs Boson*, and its role as a mass mechanism to the gauge bosons.

2.1 Spontaneous Electroweak Symmetry Breaking

The electromagnetic interaction is one of the simplest gauge theories which predict the massless photon through the classical Maxwell equations making it a long-range force [100]. The strong interaction is a short-ranged force due to the confinement of massless gluons. As for the weak interaction, even though it is also a short-range force, it doesn't have the same properties as the strong interaction. The interaction is caused by a different mechanism called **Spontaneous Symmetry Breaking** [100].

In 1961, Physicist Sheldon Glashow made tremendous progress in explaining the unsolved symmetry breaking of the electroweak theory, where he proposed an extended model with a larger symmetry group, $SU(2) \times U(1)$, and a fourth gauge boson initially called, Z_0 [60]. He postulated that there exists a mechanism that produces a boson, γ, that conserves parity and three bosons, $W^{\pm}$ and Z_0 that violate parity [60]. Along with collaborators Abdus Salam and Steven Weinberg, the unified electroweak theory became known today as the Glashow-Weinberg-Salam Theory. They were awarded with a Nobel Prize in 1979.

However, attempts to develop a gauge invariant theory for the Electroweak theory had consistently failed, and gauge theories started to gain a bad reputation. The main problem was that in order to maintain symmetry in the gauge theory, the force carriers of electromagnetic and weak forces should have zero mass. That statement, which is true for photons does not hold for the $W^{\pm}$ and Z bosons [39]. This led to confusion whether gauge invariance was an incorrect approach or there exists another mechanism that gives the particles their mass. This observation led the physics community to suggest a theory explaining the phenomena. Due to the discovery of electroweak symmetry, physicists considered the possibility that a symmetry law might not always be followed under certain conditions. In 1962, physicist Philip Anderson wrote a paper suggesting the possibility of symmetry breaking in particle physics as a solution to the problem of satisfying requirements for gauge invariance [4]. This idea paved the way to the discovery of the first scalar gauge boson in the Standard Model, the Higgs Boson.

2.2 Role of the Higgs Boson

In the mid 1960's, physicists started determining the conditions for spontaneous electroweak symmetry breaking. At that time it was hypothesized that an unusual type of field existed in order for the fundamental particles to acquire mass. One of the key features of the undiscovered field at that time was it would take less energy for the field to have a non-zero expectation value [93]. This was one of the first proposals which aimed to explain how the gauge bosons of the weak force accumulate mass under the gauge theory.

In 1964, Robert Brout and François Englert in Brussels, Peter Higgs at the University of Edinburgh, and other theorists proposed a model well known as the Brout-Englert-Higgs (BEH) mechanism [60]. The features of the mechanism include that it can give mass to elementary particles while retaining the structure of their original interactions. Importantly, this structure ensures that the theory remains predictive at very high energy [94]. Particles that carry the weak interaction would acquire masses through their interaction with the Higgs field, as would all matter particles [63]. The photon, which carries the electromagnetic interaction, would remain massless. After the universe expanded and cooled, particles interacted with the Higgs field and this interaction gave them mass [48]. The BEH mechanism implies that the values of the elementary particle masses are linked to how strongly each particle couples to the Higgs field, which is not predicted by current theories [97]. From the mechanism it could also be inferred that the new field is realized through another particle with an unknown mass.

Researchers at the time restricted the mass to be lower than 1 TeV, which was then beyond the limits of accelerators. This particle was later famously known as the Higgs boson and became the most sought-after particle in all of particle physics [48].

The Birth of the Large Hadron Collider

The Large Electron-Positron collider (LEP), which operated at CERN from 1989 to 2000, was the first accelerator to have significant reach into the potential mass range of the Higgs boson . Though LEP did not find the Higgs boson, its significant contribution in the search was determining the lower bound of the mass at 107.9 GeV at 95% Confidence Level (CL) [3]. In 1984, a few physicists and engineers at CERN were exploring the possibility of installing a proton-proton accelerator with a very high collision energy of 10-20 TeV in the same tunnel as LEP[48]. This new accelerator, called the Large Hadron Collider (LHC), could probe the full mass range for the Higgs, given there is a substantial level of luminosity. Luminosity is defined as the number of events/per area/per time. Hence, the higher the luminosity the higher likelihood for proton-proton collisions to occur [44]. However, having a high luminosity implies that each interesting collision would be accompanied by tens of background collisions. Given the state of detector technology of the time, this situation came as a challenge, which made CERN launch a Research and Development program focused on detector technology. The product of the RD Program yielded the well-known international collaborations such as ATLAS, CMS, LHCb and other LHC experiments.

On the theory side, the 1990's saw much progress: physicists studied the production of the Higgs boson in proton-proton collisions and all its different decay modes [43]. The detectors were tasked with the challenge to measure all possible kinds of particles because of the Higgs' predicted wide mass range, as the decay modes depend strongly on the unknown mass of the Higgs boson. The decay modes were studied through simulations and the important Higgs decay modes were used as a benchmark to design the detector. On the other hand, the Fermi National Accelerator Laboratory (Fermilab) in the United States is known for the Tevatron Collider. The collaboration started searching for the potential Higgs Boson and predicted the particle to have a mass around 160 GeV [43]. However, the proton-antiproton accelerator ceased operations in 2011.

In September 2008, the construction for the LHC was completed and CERN prepared its detectors for the first beams. With the international press and authorities present at the huge event, the machine worked and the collaborations

had high hopes of producing results. Unfortunately, a few days later, a problem occured in the superconducting magnets which caused major damage to the LHC. It would take a year of repairs and installation of a stronger protection system. The collaboration was then faced with a tough decision of waiting for a year to enable the LHC to work at a full capacity of 13 TeV or immediately start and operate at a lower center of mass energy of 7 TeV. Since intensive simulations showed the possibility of discovering the Higgs Boson at a lower energy, the collaboration decided to run at 7 TeV [48].

The Hunt and Discovery of the Higgs Boson

Since Higgs bosons are considered rare events, and the LHC was especially made to detect them, sophisticated analysis techniques are required to detect the signal events from the large backgrounds coming from other processes. After processes passing the criteria are identified as signal events, powerful statistical methods are used to determine the significance of the signal. Since statistical fluctuations in the background events could be mistaken as signals, strict statistical requirements are imposed before a new signal is considered relevant. The significance is quantified in terms of sigmas, σ, or the number of standard deviations of a normal distribution. In particle physics, a significance of 3σ is referred to as evidence, while 5σ is referred to as an observation, corresponding to the probability of a statistical fluctuation from the background of less than 1 in a million [5].

After data taking, physicists soon analyzed the data. In the summer of 2011, there were a few excess events in the Higgs decay mode to two W bosons at a mass approximately 140 GeV. Furthermore, another excess of events at the same mass was observed in another decay mode, a Higgs decaying to two photons, also called the diphoton channel [43]. However as more data were taken and analyzed, the excess of events decreased. By the end of 2011, ATLAS had collected and analysed 5 fb^{-1} of data at a center-of-mass energy $\sqrt{s} = 7$ TeV. After combining all of the decay modes, physicists were able to constrain the mass of the Standard Model Higgs Boson to be around 125 GeV, where an excess of 3σ is observed through the diphoton and four lepton decay modes [48]. Although these results were signficant enough for evidence and not an observation, it was a great progress since both ATLAS and CMS experiments had excess of 3σ at the same mass.

In 2012, the center-of-mass energy of the LHC increased from $\sqrt{s}$ =7 TeV to $\sqrt{s} = 8$ TeV, which increased the cross-sections for Higgs boson production. ATLAS collected another 5 fb^{-1} at $\sqrt{s}$ 8 TeV, which doubled the data set [48]. After analyzing the set of data, the significance of the bump continued to increase. The joint seminar with the major experiments, ATLAS and CMS, last

July 4, 2012 caused excitement around the physics community especially after the confirmed attendance of François Englert and Peter Higgs. In the seminar the two collaborations showed their results, which was finding an excess of 5σ at a a mass of 125 GeV. This event was famously known as the discovery of the Higgs-like particle.

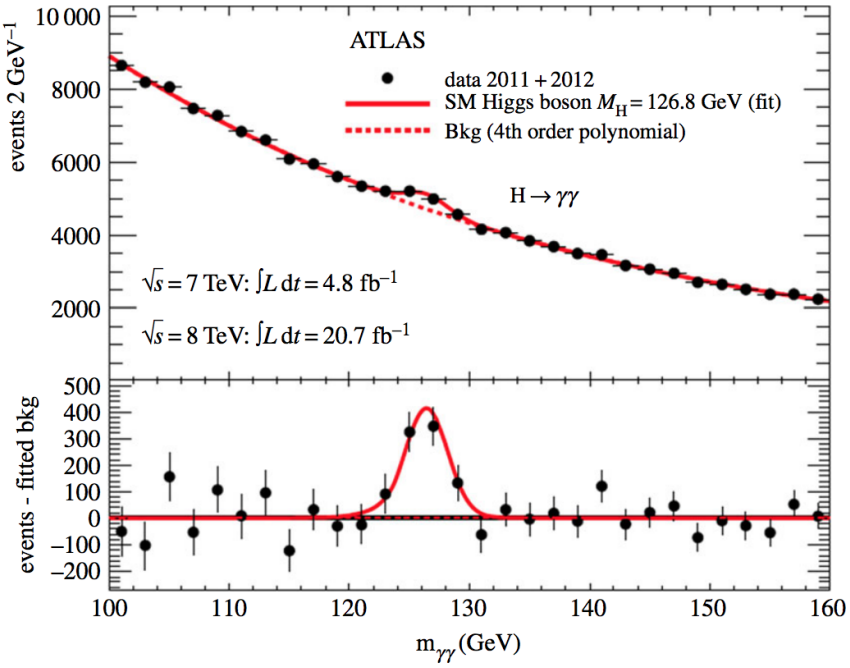

Figure 7: Plots showing the observation of a new particle at 5σ [25]

In Figure 3, the top plot describes the fit to the exponential background superimposed with the sum of signal and background events. While the bottom plot displays the residuals of the data with respect to the fitted background events.

Aftermath

After the discovery of the higgs-like particle in 2012, physicists began an intensive study in understanding the properties of the scalar Boson to determine the mechanism, decay modes, and the type of Higgs boson. The newly discovered particle is unique in the standard model because it has zero-spin, no electric charge, and no strong force interaction. Unanswered questions have opened in regards whether there is only one Higgs boson or there is more than one.

In summary, one of the main takeaways with the interaction of the Higgs boson with other Standard Model particles is to compare the interaction strength to the mass of each particle. As discussed earlier, one of the main predictions of the BEH mechanism in the Standard model was that the interaction strength depends on the particle mass. For example, the heavier the particle, the stronger

its interaction with the Higgs field. Aside from verifying the properties of the Higgs boson that is predicted by the Standard Model, opportunities for searching for Physics Beyond the Standard Model (BSM) is another goal of physics analyses at the LHC. Theories had been laid out which give an assessment of the potential decay modes which will be discussed in further detail in Chapter 3.

3 Physics Beyond the Standard Model

The discovery of the Higgs-like particle at 125 GeV in 2012 was a tremendous success for both theoretical and experimental particle physicists. The Higgs boson has played an important role in explaining unanswered questions in the Standard Model but at the same time has opened the opportunity to make use of the physics analyses in the LHC to find evidence for new Physics. As one of the most recently discovered scalar particles, there are unanswered questions about the kinematics and decay modes of the Higgs Boson. An extensive survey of possible decay modes to guide experimental analyses in the LHC laid out different theories of higgs decay modes [34]. The paper gives a literature review of the theories, defines simplified models, sets constraints, and assesses potential for discovery. This chapter discusses the motivation of the research and one of the theories from that paper.

3.1 Motivation of Exotic Higgs Decays

A rich experimental program was developed to study the precise measurement of the Higgs Boson's couplings to Standard Model particles. The focus of the theory paper [34] is to search for *exotic* decays, where "exotic" meant decays that are forbidden in the SM or predicted to occur with a suppressed branching fraction [16]. With a growing extensive literature, exotic Higgs decays are a potential option in understanding BSM by utilizing the LHC. However, searching for these decays pose a challenge since they are currently unconstrained by other existing analyses.

Narrow Width (Γ): The SM Higgs Boson has a narrow width of $\Gamma \cong 4.07$ MeV. Decay width is expressed in terms of a lifetime of a particle, or simply $\Gamma \propto \frac{\hbar}{\tau}$, which is a measure of the probability of a specific decay process occurring within a given amount of time [52]. A narrower decay width implies that the particle's lifetime is longer. Hence, the Higgs Boson has a higher probability of coupling with to other light states in both SM and BSM [35]. Therefore, there are decay modes worth exploring.

Higher Precision of Branching Ratios ($H \rightarrow BSM$): The theory paper presented that from the data analyzed from the LHC for run 1 at center-of-mass energies $\sqrt{s} = 7$ and 8 TeV, a branching ratio of $\mathrm{Br}(h \rightarrow BSM \leq 20\%)$ at 95% Confidence Level (CL) could be assumed for Higgs decaying to BSM particles. The branching ratio seems large from the analysis, but with the LHC operating at a higher luminosity suggests future prediction with higher precision of $\mathrm{Br}(h \rightarrow BSM \leq 5\%)$ at 95% CL [35]. The branching ratio is the fraction of time

a particle decays to a particular final state, $Br(Process) = \frac{\Gamma_i}{\Gamma_{tot}}$ [52]. However, particles could have more than one decay mode. The current branching ratio of Higgs decaying to BSM particles at the LHC indicates a potential possibility. Future upgrades for the LHC would improve the precision of the predicted branching ratio.

The main takeaway: Since all the decay modes of the Higgs boson are not fully accounted for, the possibility of exotic higgs decays cannot be excluded yet. Especially hardware and high-luminosity upgrades would improve the sensitivity of the LHC to lower branching ratios and probe BSM decay modes.

3.2 SM + Vector

Various BSM theories feature a "hidden" or "dark" sector of matter that does not interact directly with SM particles but could interact weakly with SM matter by coupling to the Higgs field [29]. In this theory there are two types of portals that could address the dark-matter problem providing two types of decays: **Hypercharge Portal** and **Higgs Portal** [33]. These portals provide kinetic $Z - Z_D$ mixing through the decay $H \to ZZ_D$ and higgs $H - H_D$ mixing through the decay $H \to Z_D Z_D$ and $H \to ss$, which are regulated by small coupling parameters such as ϵ and κ [33]. There are two vector-boson mass eigenstates, Z_D and the SM Z boson, and two scalar mass eigenstates, s and the SM H boson. Hence, the possible physical (mass) states in the theory are denoted by H, s, Z and Z_D [29].

The model this research is focusing on is the Higgs Portal in which there exists a $U(1)_D$ symmetry in the dark sector. The dark vector gauge boson Z_D, or known as the "dark photon," is given mass through the scalar field s, that also breaks the symmetry in the dark matter sector and is analogous to the Higgs field H, in the visible SM sector [33]. The next section explains a description of the decay process studied in the research in detail.

3.3 H $\to Z_D Z_D \to$ 4l

The SM + V theory allows for different types of exotic higgs decays and there are two connections between the dark and the SM sectors: kinetic mixing ϵ and higgs mixing κ. The regime depends on which type of mixing dominates [33]. Given the analogous broken $U(1)_D$ in the dark matter sector, kinetic mixing dominates when $\epsilon >> \kappa$ and the exotic decay mode $H \to ZZ_D$ occurs as shown in Figure 9. On the other hand, this research focuses on the other type of mixing regime where the higgs mixing dominates ($\kappa >> \epsilon$) and the exotic decay mode $H \to Z_D Z_D$

and $H \to ss$ occurs as shown in Figure 10 and Figure 11, respectively [33].

Using existing LHC datasets at 7 and 8 TeV, Curtin's exotic Higgs decay group used the previous run data to constrain the mass of the dark photon (Z_D) [35]. As shown in Figure 8, the mass plane in the SM + V model with different exotic Higgs decays for $\kappa >> \epsilon$. The black contours are ranges of values of $\kappa \times 10^3$ required for $\text{Br}(h \to Z_D Z_D, h \to ss) = 10\%$ [33]. Region A is the SM + V Sector which shows that the dominant exotic higgs decay is $h \to Z_D Z_D$ (the dotted red line indicates $m_h = m_s$). On the lower left, Region B has both $h \to ss$ and $h \to Z_D Z_D$ decays. On the upper right, Region C has no exotic Higgs decays while on the lower right, Region D reproduces the SM+S model (Not a focus of this thesis). Focusing on Region A in Figure 8, the dominant exotic higgs decay $h \to Z_D Z_D$ occurs when the mass of the dark photon is between $\mathbf{0 \leq m_{Z_D} \leq 60}$ GeV.

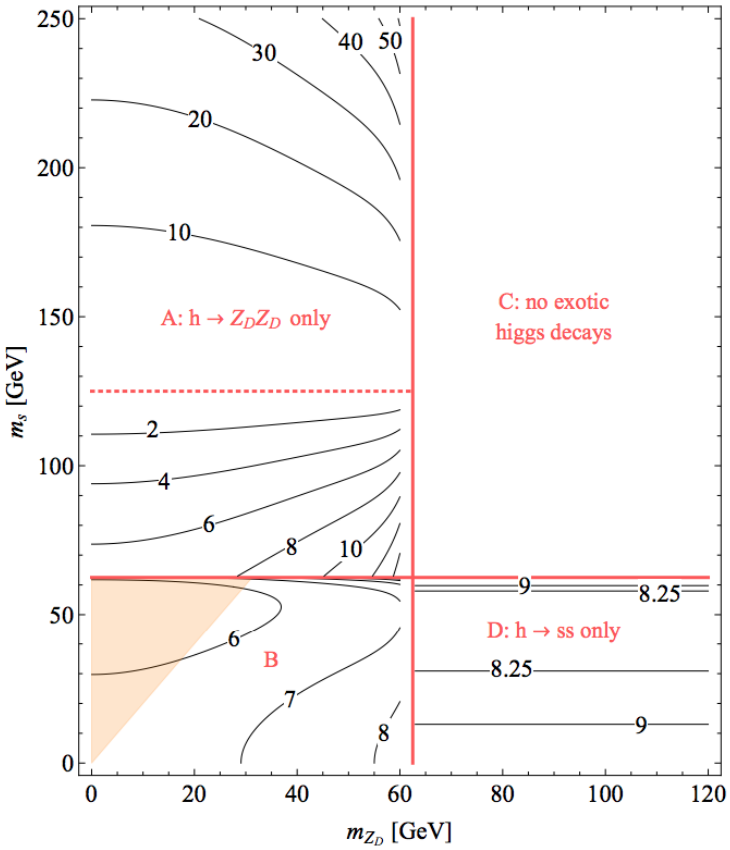

Figure 8: Decay Modes Under SM + V Theory [33]. Region A is the region where $h \to Z_D Z_D$ is the dominant decay, where the red dotted line is when $m_s = m_h$. Region B shows when the following decays occur: $h \to ss$ and $h \to Z_D Z_D$ (Theory not considered in this thesis), Region C has no predicted decays, and Region D shows that the decay $h \to ss$ occurs (Theory also not considered in this thesis). The black contours is the parameter $\kappa \times 10^3$ required for the $\text{Br}(h \to Z_D Z_D, ss) = 10\%$

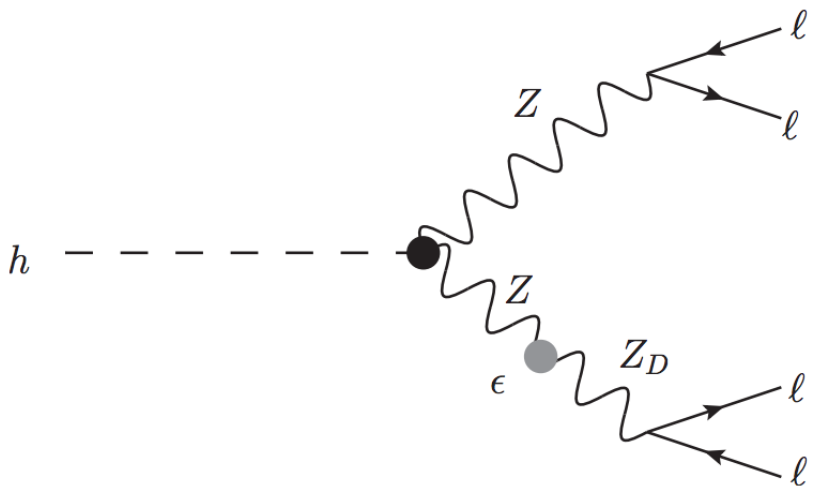

Figure 9: Dominant Exotic Higgs Decay under Kinetic Mixing [37]

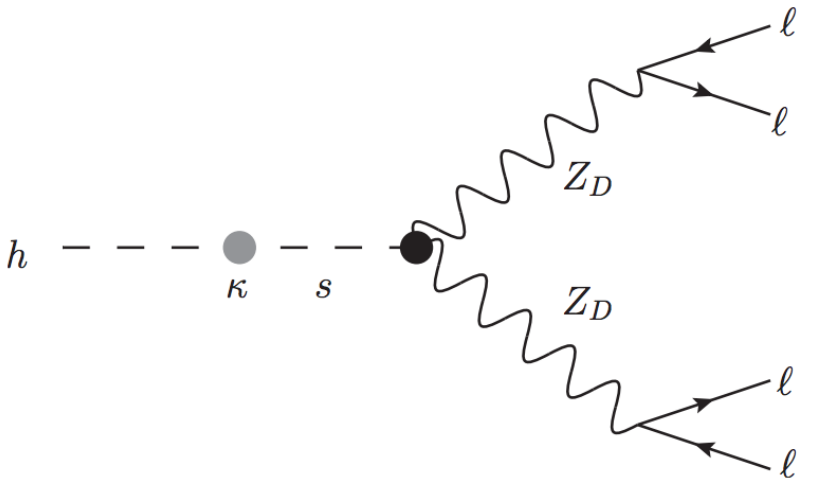

Figure 10: One Type of Exotic Higgs Decay under Higgs Mixing [37]

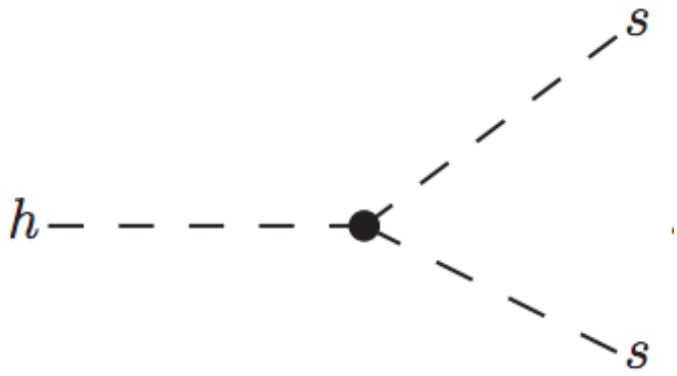

Figure 11: One Type of Higgs Decay under Higgs Mixing [33]

4 ATLAS Experiment

ATLAS (A Toroidal LHC ApparatuS) is one of the four major experiments at the Large Hadron Collider (LHC) at CERN in Switzerland. It is a general-purpose particle physics experiment that is led by an international collaboration which makes use of precision measurement to seek answers to fundamental questions. Physicists under the experiment test the predictions of the Standard Model, which explains current understanding of the building blocks of matter and their interactions. ATLAS was one of the two LHC experiments that lead the groundbreaking discovery of the Higgs boson and is currently involved in searching for physics beyond the Standard Model.

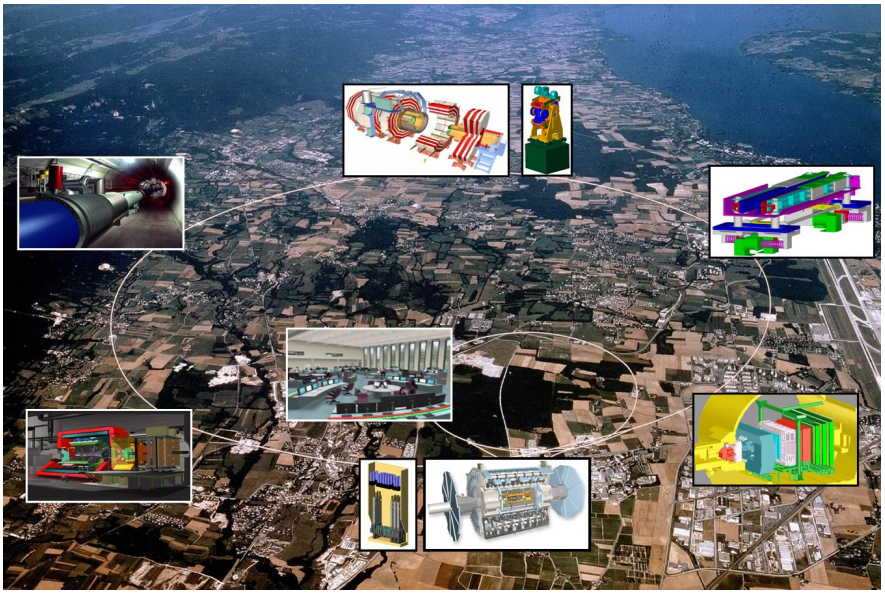

Figure 12: Major LHC Experiments [22]

Brief History

It all began with the birth of LHC project in 1991, it was followed by an extensive research to determine the type of technologies necessary for the project to come to realization. The following year, in the LHC Experimental Program meeting in Evian-les-Bains, physicists gathered to propose experiments for the LHC [23]. Two smaller collaborations proposed an experiment based on a large toroidal magnet system. The two research groups soon merged and became known as the ATLAS collaboration. After sending a letter of intent, submitting a technical proposal of the experiment, and adhering to subsequent edits and reports, the committee and CERN's Director-General Chris Llewellyn Smith officially approved the construction of the ATLAS detector in 1997 [23] . ATLAS teams immediately started developing and building detector components. Nearly ten years after being approved for construction, in November 2006, the ATLAS barrel toroid was switched on for the first time and was considered the largest superconducting

magnet at that time. Along with two endcap toroids and solenoid magnet, these components work together to bend paths of charged particles produced in the collisions [23]. Towards the end of 2008, the construction of the ATLAS detector was finally finished and data acquisition began the following year. Since then, the experiment has garnered recognition through its discoveries and is currently in a long shutdown for upgrades to increase total energy to 14 TeV in its future operations.

Currently, the ATLAS collaboration is comprised of around 3000 scientific authors from 183 institutions around the world, representing 38 countries from all over the world [23]. It is considered one of the largest collaborative efforts in science. With such a challenging project, the required intellectual and financial resources needed in order to maximize scientific output is met by establishing an international effort. This chapter aims to further discuss the specifics of the mechanics of the detector and its important components.

4.1 The ATLAS Detector

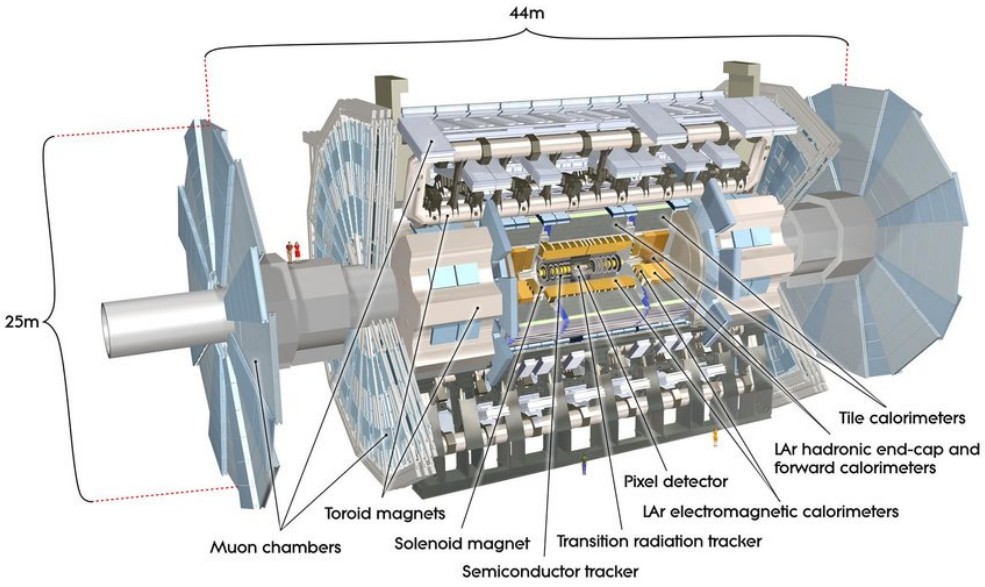

Figure 13: ATLAS Detector [24]

As shown in Figure 5, The ATLAS detector is 44 metres long, 25 metres in diameter, and weighs around 7,000 tonnes. The detector can be divided into four major parts: the Inner Detector, the Calorimeters, the Muon Spectrometer and the magnet systems. The Inner Detector tracks particles precisely and is sensitive because it's close to the interaction point [91], the calorimeters measure the energy of charged particles [91], and the muon spectrometer identifies and measures

momenta of muons [91]. The two magnet systems bend charged particles in the Inner Detector and the Muon Spectrometer, which allows an accurate measure of particle momentum.

Most particles can be detected aside from neutrinos. Even though neutrinos are stable, they only interact through the weak interaction and do so only rarely. Therefore, neutrinos are detected using an indirect method by measuring a momentum imbalance among detected particles [91]. In order to efficiently detect neutrinos, the detector must be able to detect all non-neutrinos. Hence, the detector must be maintained for high performance under radiation.

4.1.1 Inner Detector

Since the inner detector is close to the interaction point, it is the first component of the detector to observe the decay products of the proton-proton collisions [46]. Hence, it is compact and highly sensitive. It consists of three different systems of sensors all immersed in a magnetic field parallel to the beam axis to accurately measure the direction, momentum, and charge of charged particles produced in each collision [40]. The main components of the Inner Detector are: **Pixel Detector, Semiconductor Tracker (SCT), and Transition Radiation Tracker (TRT)**.

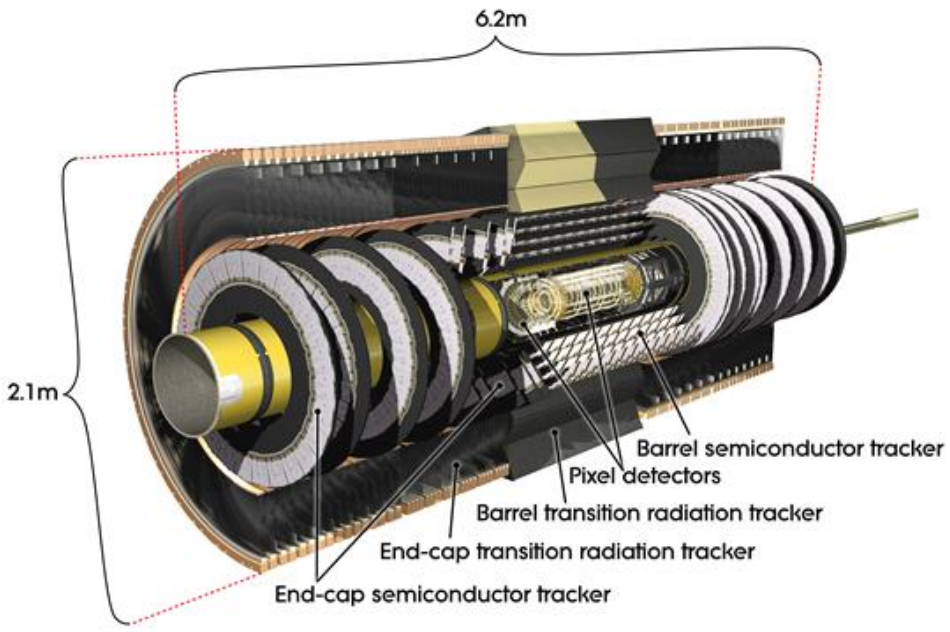

Figure 14: Inner detector showing the pixel detector, semiconductor trackers, and transition radiation trackers [91]

Pixel Detector is located in the innermost part of the detector. The basic unit of the pixel detector is the module. A module is a rectangular active device

approximately 6cm by 2cm with 46,080 pixels, each 50 μm by 400 μm along the beam (Garcia-Sciveres, 2002, p. 1). All modules are identical and are arranged in three concentric cylinders along the beam axis with three disks at each end cap of the barrel. The detector has 1,456 barrel modules and 288 disk modules making it a total of 1,744 modules and each contains 16 readout chips and other electronic components [42]. Furthermore, the detector is designed to have high precision tracking close to the interaction point to acquire the surge of data after proton-proton collisions. A beam in the LHC is not a continuous string of particles, but rather divided into chunks called *bunches* a few centimetres long at the collision point [44]. Each bunch contains about a hundred billion protons and when bunches collide, a number of proton-proton collisions occur. The current beam collision rate at the LHC will be 40MHz or 25 ns with multiple interactions per bunch crossing, and the detector must be able to resolve data from each crossing [42]. In order to operate at such high rate every pixel must be read out by an independent electronics channel. In total, the Pixel Detector has over 80 million readout channels, 67 million channels in the barrel and 13 million in the disks [55]. Having a large readout channel count to accommodate data from each collision poses a design and engineering challenge. Furthermore, another challenge is the detector's exposure to radiation due to its close proximity to the interaction point. The situation required all components to be radiation hard in order to endure significant radiation levels during operation.

The Semi-Conductor Tracker (SCT) is the middle component of the inner detector. It is similar in concept and function to the Pixel Detector but it is composed of long, narrow strips instead of small pixel modules. The microstrip detector modules are the key elements of the Semiconductor Tracker, as they will measure track coordinates with high precision [27]. The silicon microstrip tracker consists of 4,088 two-sided modules and over 6 million implanted readout strips with each having the dimensions 80 μm by 12 cm [96]. The SCT is the most critical part of the inner detector for basic tracking in the plane perpendicular to the beam, since it measures particles over a much larger area than the Pixel Detector [27].

The Transition Radiation Tracker (TRT) is the outermost component of the inner detector and provides additional information on the particle type that flew through the detector. The TRT is a combination of a straw tracker and a transition radiation detector. The TRT contains 350,000 read-out channels, 50,000 straws in the Barrel with each straw 144 cm long. On the other hand, the endcaps have 250,000, each straw is 39 cm long [76]. However, even though

the TRT is less precise compared to the other two detectors, it was necessary in order to cover a larger volume and to have transition radiation detection capability. Each drift tube is filled with gas that becomes ionized when a charged particle passes through in order to produce a current pulse in the wire [57]. The wires containing the signals then create a pattern of each "hit" which determines the path of the charged particle. The drift tube contains materials like Xenon and Argon gas with different indices of refraction, which causes ultra-relativistic charged particles to produce transition radiation and leave stronger signals in the straws [75]. Lighter particles have higher speed. Hence, particle paths that contain strong signals are identified as light charged particles like electrons.

4.1.2 Calorimeter

The calorimeters are located outside the solenoid magnet and measure the energy a particle loses as it passes through the detector. There are two types calorimeter systems: an **electromagnetic calorimeter** and an **hadronic calorimeter** [46]. The calorimeters absorb energy in high-density metal and periodically sample the shape of the resulting particle shower, inferring the energy of the original particle from this measurement[88].

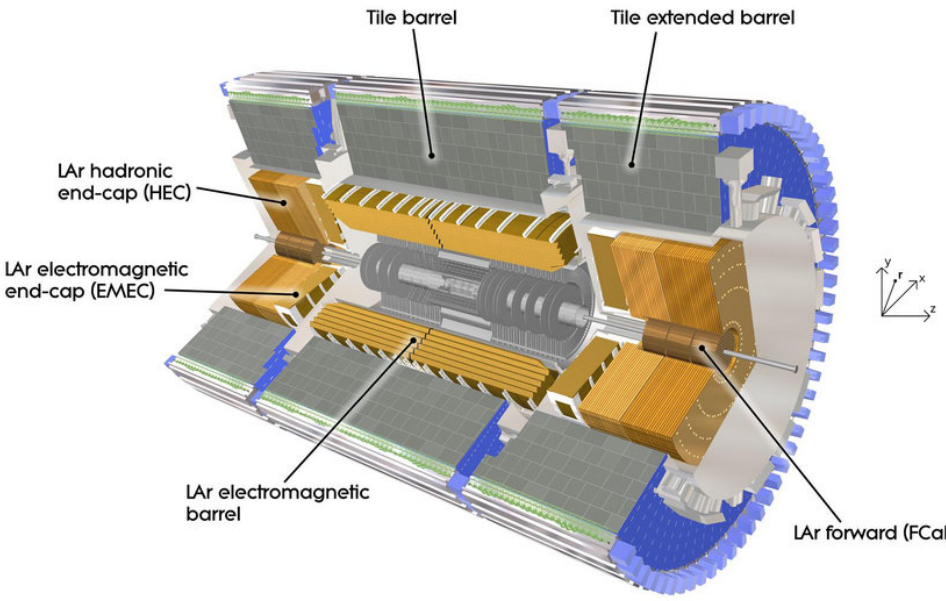

Figure 15: Electromagnetic and Hadronic Calorimeters along with other components [91]

Electromagnetic calorimeters measure the energy of electrons and photons as they interact with matter [56].

Hadronic calorimeters sample the energy of hadrons (particles that contain quarks, such as protons and neutrons) as they interact with atomic nuclei. Calorimeters can stop most known particles except muons and neutrinos [56].

4.1.3 Muon Spectrometer

Muons are second generations leptons that arise out of the decay of particles produced by the collision of protons in the center of the ATLAS detector. The muons' signals enable inferences about which particles came out of the impact of the protons. Since muons are not stopped at the calorimeter, then physicists built the muon spectrometer. It is the outermost part of the ATLAS detector and measures the energy and trajectory of the muons with high accuracy [91]. To this end, the particles are deflected in a strong magnetic field generated by superconducting magnetic coils.

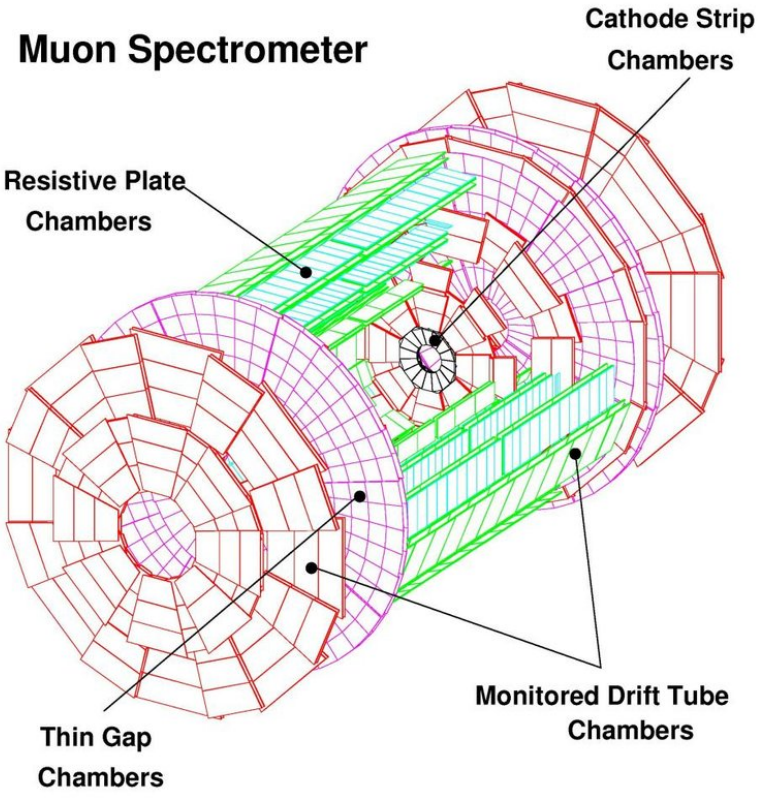

Figure 16: Muon Spectrometer components [91]

In order to measure the muon tracks, the physicists use muon drift tube chambers (MDT) [8] which consist of several layers of drift tubes filled with a gas mixture [85]. Muons interact with the argon atoms leaving tracks in the drift tubes. Using a high voltage of 3000 V between the tube wall and central counting wire, the tracks are registered and converted into electronic signals [85]. The muon spectrometer is the reason behind the ATLAS detector's large size. The spectrometer

contains 1,150 MDT chambers and 350,000 drift tubes which measures the paths of the muons that pass through [27].

4.1.4 Magnet System

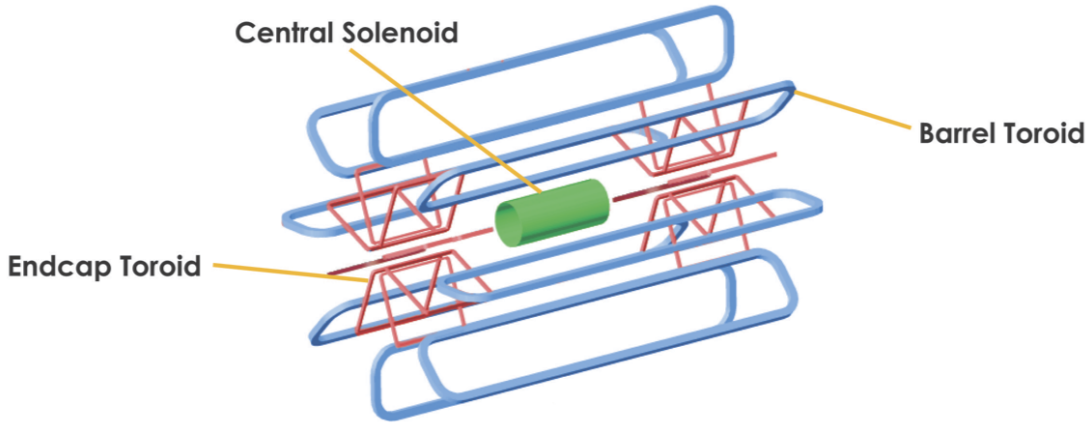

Figure 17: Magnet System [26]

The magnet system of ATLAS bends particles around the various layers of detector systems, making it easier to contain the tracks of particles. The main sections of the magnet system are: **Central Solenoid Magnet, Barrel Toroid and End-cap Toroids** [45].

The ATLAS detector uses two large superconducting magnet systems (inner and outer solenoid) to bend charged particles to accurately measure particle momenta. Going back to electromagnetism course, the bending of particles is due to the Lorentz force, which is proportional to velocity. Since all particles produced in the LHC's proton-proton collisions are traveling at very close to the speed of light, the force on particles of different momenta is equal (Kate, 1999, p. 841). Thus high-momentum particles curve very little, while low-momentum particles curve significantly. The particle momentum is then calculated from the particle's curvature.

The Central Solenoid produces a 2 Tesla magnetic field surrounding the Inner Detector. The high magnetic field allows particles to bend and consequently determine their momentum [59]. However, particles with momenta below a certain threshold would curve very strongly so that they would loop repeatedly in the field and wouldn't be measured. On the other hand, the outer toroidal magnetic field is produced by eight large superconducting barrel loops and two endcaps toroidal magnets situated outside the calorimeters and within the muon system [47].

4.2 Trigger System

ATLAS is designed to observe billions of proton-proton collisions per second, with a combined data volume of more than 60 million megabytes per second. However, only a few of these events will contain interesting characteristics that have the potential to lead to new discoveries [101]. To reduce the flow of data to manageable levels, ATLAS uses a complex two-level online event selection system called the **Trigger System** [74]. The trigger selects events with strict parameters which are considered interesting for physics analyses. The ATLAS trigger system carries out the selection process in two stages: **Level-1 Hardware** and **Level-2 Software Trigger Systems**.

Level-1 Hardware Trigger is constructed with custom-made electronics and works on a subset of information from the calorimeter and muon detectors [74]. The run time of the decision to keep the data from an event is $2.5\mu s$ and the Level-1 trigger reduces the interaction rate from 1 GHz to 75 kHz [101].

Level-2 Software Trigger refines the analysis of the hardware-based Level-1 trigger. It conducts a very detailed analysis either by performing overall examination of the whole event for selected layers of the detector, such as calorimeters, trackers, muon detectors and by utilizing the data in smaller and isolated regions of the detector [74]. Approximately a few hundreds of events per second are selected for permanent storage and subsequent analysis discarding most of the abundant low-momentum interactions [82]. The Level-2 Trigger System reduces the interaction rate from 75 kHz to 1 kHz [101].

5 Data, Simulated Samples, and Event Selection

The ATLAS Collaboration analyzed proton-proton collision run 2 data, collected at the LHC during 2016, with a center-of-mass energy of $\sqrt{s} = 13$ TeV and integrated luminosity of $\mathcal{L}_{int} = 32.9 fb^{-1}$ [29]. A rigorous event selection criteria was developed to determine what processes are considered to be signal and background events. This chapter discusses the event selection criteria in detail and the Monte Carlo (MC) simulated events for both SM and BSM data for the predictive study.

5.1 Signal and Background Sample Data

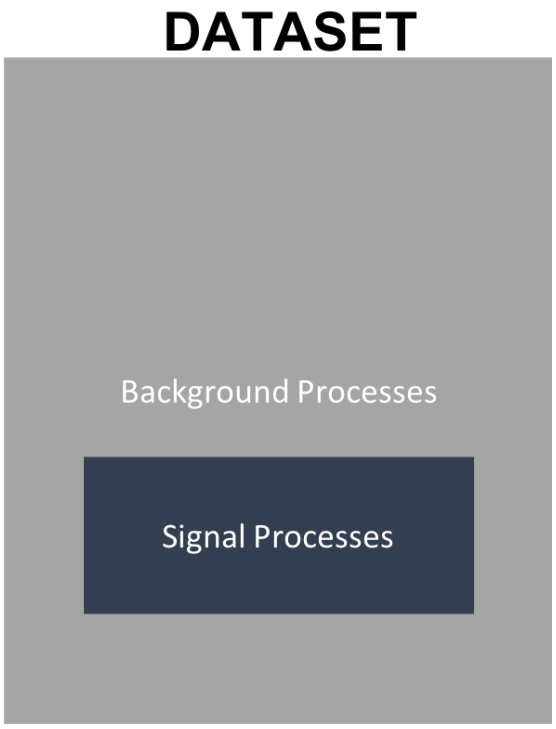

Figure 18: Illustration of Background and Signal Data

Consider a dataset shown in Figure 18, within that data there exist various processes. **Signal Data** corresponds to the particular process of interest in the study. On the other hand, **Background Data** are also processes that might be similar to the signal but are not. The selection criteria in determining which signals are considered for the study are discussed in more detail later in the chapter. Aside from the SM Signal and Background Data, simulated data are also produced for chosen BSM Processes. Determining signal and background processes are important especially when searching for rare events or faint signals. Background processes contribute to the number of observed events, and the presence of excess events could potentially be attributed to the faint signal. Through statistical methods, physicists then determine the significance of the signal.

5.2 Event Selection Criteria

From the survey of exotic higgs decay processes, the analysis was divided into two regimes: the **heavy Z_D case** with **10 GeV $< m_{Z_D} <$ $\frac{m_h}{2}$ GeV** (where m_h is the mass of the Higgs Boson), and the **light Z_D case** with **2μ GeV $< m_{Z_D} <$ 10 GeV** . This thesis focuses on the heavy Z_D analysis, where the elements are divided according to all possible flavor composition combinations of the four lepton state: $4e$, 4μ, and $2e2\mu$ [36]. The feynman diagram in Figure 6 Chapter 3 showed the process of $H \to Z_D Z_D \to 4l$, where l stands for leptons. In Chapter 1, leptons could be either charged or uncharged (neutrinos), and are classified into electrons, muons, and taus. In this particular study, the process decays into four muons or 4μ.

A particle's coupling strength to the SM Higgs Boson is proportional to its mass. Even though the study focuses on the heavy Z_D mass, its mass is low enough making the dark vector boson's coupling with the SM Higgs to be weak. Weak couplings decay slower compared to particles with a strong coupling. Particles that decay slower after the primary proton-proton collisions are called long-lived particles (LLP). Hence, Z_D is a LLP and decays slower compared to the SM Z Boson. A candidate signal events are then selected by identifying the opposite charged muon pairs, $\mu^+\mu^-$, that were produced at a vertex displaced within several centimeters from the primary proton-proton collision, or also known as Interaction Point (IP) [29]. The goal of the selection criteria is to suppress the background from SM processes (e.g $H \to ZZ$) that produce muons near the primary collision point while at the same time efficiently accepting signal events over a wide range of LLP masses, lifetimes and velocities [29].

5.2.1 Trigger Requirements

In Chapter 4, the Trigger of the ATLAS detector has two stages, the hardware and software systems. Establishing a concrete trigger system is important to discriminate between the background and signal processes. For example, $H \to ZZ \to 4l$ is a common process predicted in the SM where the SM Z boson also decays to 4 leptons. Hence, this process is similar to $H \to Z_D Z_D \to 4l$ because the final state also consists of four leptons. As discussed in section 5.2, the coupling strength of the SM Z boson is stronger compared to the dark vector boson Z_D. Therefore, one major difference is that the SM Process decays faster so the muon pairs are produced at a vertex nearer from the IP (prompt vertices). Hence, events must satisfy the requirements of the trigger for the dark sector model in order to differentiate between processes and achieve optimum signals.

- Level-1 Hardware Trigger: is based on reconstruction of muon tracks with low transverse momentum (p_T) thresholds, such as $p_T > 10GeV$. The large rates associated with the low p_T thresholds are offset by requiring that pair of muons detected in the Muon Spectrometer have a small angular separation, such as $\Delta R < 0.5$ [29].

- Level-2 Software Trigger: uses algorithms that loop over all the events to select which satisfy the requirements. For example, the muon reconstruction algorithm extrapolates the trajectories of the muon tracks from the IP. The muon tracks generated in the process are identified and can either be accepted or rejected from the method [29].

  Main Takeaway: The Trigger system has designated certain cuts in observables such as p_T and ΔR to ensure the signal data do not overlap with other processes that have muons in the final state.

5.3 BSM Signal Samples

5.3.1 Previous ATLAS Paper

Monte Carlo simulated samples from the BSM physics model were used to determine the selection criteria and to calculate the signal efficiency to convert signal upper limit into cross-section upper limit [29]. The chosen model, the dark-sector gauge boson model featuring the dark photon, Z_D, opens a variety of BSM physics possibilities and kinematics. Samples for the models were generated with MadGraph5_aMC@NLO [6], a framework that provides elements needed for BSM phenomenology. Five signal samples were generated with Z_D masses and lifetimes shown in Table 2. The Higgs boson is produced via the gluon-gluon fusion process, assuming a cross-section of 44.1 pb.

m_{Z_d}(GeV)	cτ (cm)	Br($Z_D \to \mu^+\mu^-$)
20	50	0.1475
40	50	0.1370
40	500	0.1370
60	50	0.1066
60	500	0.1066

Table 2: MC signal samples for the dark-sector model. For all samples, $m_H = 125$ GeV, $\sigma(pp \to H) = 44.1$ pb and Br$(H \to Z_D Z_D) = 0.10$ [29]

Gluon-Gluon Fusion Process

In Chapter 3, there are two possible decays under Higgs mixing: $H \to ss$ and $H \to Z_D Z_D \to 4l$. An interaction exists that allows for the process $H \to ss$ to

occur, which is not discussed in this thesis. Rather it is assumed in the study that the dark higgs, s, is heavier than half the mass of the SM Higgs, H, so that the process is kinematically forbidden [37] There are various modes for Higgs production, but if $m_s > \frac{m_H}{2}$ occurs, then the dominant mode for the Higgs production process is called **gluon fusion** [37]. The cross-section, σ, of this process can be calculated and is important because in particle physics it is the probability that a given scattering process will occur [52]. In the analysis, the $\sigma(pp \to H) = 44.1$ pb was calculated from the next-to-next-to leading order term [29]. Leading order terms, also called *corrections*, within a model are the terms with the largest order of magnitude [61]. The next set of larger terms are called *next-to* leading order terms.

5.3.2 Current Study

For this thesis, since it is a predictive study for run 3, simulated MC data with similar LLP mass and lifetime from run 2 were used with the same selection criteria but scaled at an integrated luminosity of $\mathcal{L}_{int} = 300 fb^{-1}$.

5.4 SM Background Samples

5.4.1 Previous ATLAS Paper

Simulating MC data sets of background processes are considered as a guide for the selection criteria and for categorizing the types of background. The background yield is important because if an interesting signal exists then it would cause an increase in the number of selected events, and these can be compared with the predicted yield from the known background data in order to make a statistical statement about the production rate. However, if the number of observed events is close to the background prediction, then the signal of interest could be ruled out [94]. However, the selection criteria are extremely effective at eliminating background, where simulating statistically accurate background samples in the respective signal regions is very challenging [37].

5.4.2 Current Study

The BSM Background samples were supposed to be MC simulated data, however the strong selection criteria suppressed most of the background. Hence, since this thesis is a predictive study and an extrapolation from the previous ATLAS study, each of the run 2 background samples were used and scaled to correspond to an integrated luminosity of $\mathcal{L}_{int} = 300 fb^{-1}$ for run 3.

6 Data Analysis

This thesis study aims to calculate for the 95% Upper Limit of the cross section ($\sigma_S^{95\%CL,UL}$) for run 3 with an integrated luminosity of $\mathcal{L}_{int} = 300fb^{-1}$. From the signal and background samples discussed in the previous section, this chapter discusses the analysis involved for the study: scaling of the background sample, calculation of the efficiency and 95% Upper Limit of the Signal, and conversion to the 95% Upper Limit of the Cross Section.

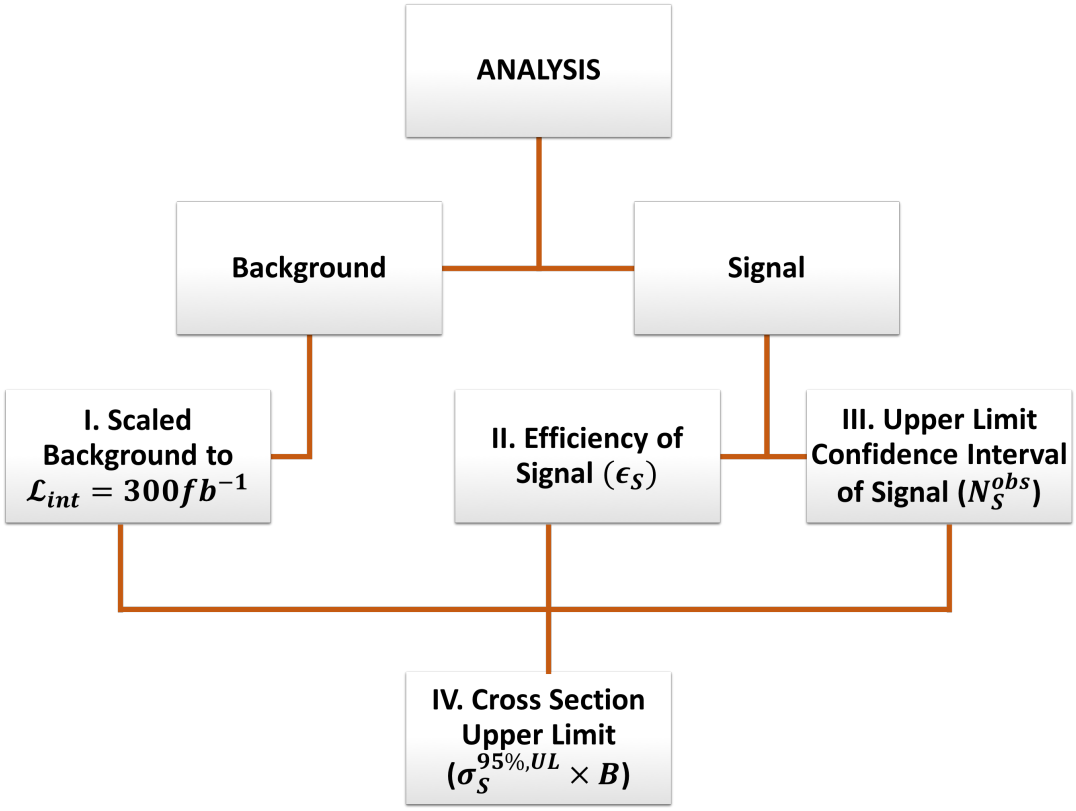

Figure 19: Diagram illustrating a brief overview of the data analysis method

From Figure 19, the data analysis is divided into two parts: the background and the signal datasets. For background data, the first step is to scale the background data to the run 3 integrated luminosity of $L_{int} = 300fb^{-1}$. Then for the signal data, the second component that needs to be calculated is the efficiency of the signal, which is the likelihood of the process of interest occurring in the dataset. The third component would be calculating for the upper limit of the signal. All these three components would be needed to calculate for the fourth and most important component for this thesis, the 95% Confidence Level (CL) cross - section Upper-Limit (UL).

6.1 Scaling of Background

Run 2 data was taken at an integrated luminosity of $\mathcal{L}_{int} = 32.9 fb^{-1}$ and the measured background using data-driven techniques was 13.8 ± 4.9 events containing a mixture of systematic and statistical uncertainties [30].

6.1.1 Uncertainties

In particle physics, one of the most important statistical methods is considering the **Uncertainty** of a variable. Also known as the margin of error of a measurement, it is a range of values that contains the true value of an observable. An uncertainty is defined by the following notation, *measured value* $\pm$ *uncertainties*. There are two types of uncertainties: the **Statistical** and **Systematic Uncertainties.**

- ***Statistical Uncertainties***: could be determined empirically from the distribution of a large sample and could be reliably estimated by repeating measurements [9]. This uncertainty could be reduced with $\sqrt{N}$ where **N** is the sample size [2]. Some examples are measurements from a poisson or binomial distribution. Using the run 2 background data, the measured value of the background could be easily scaled by $B_{meas} = \frac{300}{32.9} \times 13.8 = 125.8$ events. However, solving the statistical uncertainty would not be scaled by that ratio but rather the square root of the background itself. Hence the statistical uncertainties for run 3 would be $B_{unc} = \sqrt{N} = \sqrt{13.8 \times \frac{300}{32.9}} = 11.2$ events. Hence, the scaled background for run 3 is ***125.8 $\pm$ 11.2 events***.

  This measurement with only statistical uncertainties is called the ***Optimistic Approach*** of the study.

- ***Systematic Uncertainties:*** could only be calculated through sampling and could not be reduced with $\sqrt{N}$. Furthermore, it is more challenging to determine than a statistical uncertainty. Some examples are calibration uncertainties from the detector and limited knowledge about the background processes [9]. Using the run 2 background data,the measured value of the background (B_{meas}) remains the same, while the systematic uncertainty would also be scaled using the same ratio. This leads to $B_{unc} = \frac{300}{32.9} \times 4.9 = 44.7$ events. Hence, the scaled background for run 3 is ***125.8 $\pm$ 44.7 events***.

  This measurement with only systematic uncertainties is called the ***Pessimistic Approach*** of the study.

Data acquired from run 2 of the LHC is a combination of statistical and systematic uncertainties. Since this thesis is a predictive study, it is not possible to obtain the exact contributions of these uncertainties. Hence, calculating two measurements with only systematic and statistical uncertainties serve as a range for the true value of the scaled background events for run 3.

6.2 Efficiency (ϵ_S)

In Chapter 4, the trigger of the ATLAS detector was introduced, which is the system that carries out the selection process of interesting events for analysis. The interesting events are stored and transformed into important quantities, such as energy and momentum. This thesis' focus is studying a particular exotic higgs decay mode, hence, the only interesting events include processes that contain the corresponding final state of that reaction. A selection procedure could then be defined that loops over all events and decides whether to accept or discard a specific event. At the end of the selection, a subset from the dataset contains the sample of potential candidates. The MC simulated signal dataset discussed in Chapter 5 is considered as the complete simulation of the final states containing the particular decay mode of interest. On the other hand, the background events are categorized as processes that are not of interest but rather have similar characteristics to the particular process of interest. These categories correspond to two hypotheses: the *signal hypothesis*, H_S, and the *background hypothesis*, H_B [10]. The selection procedure is then a hypothesis test of the experiment and in order to optimize this procedure, it is applied to the MC samples. Since the background sample is scaled from the previous run data, the selection procedure was only applied to the MC simulated signal data. The two important components of the test are S_0, which is the number of total simulated events and S_f, which is the potential candidates from the selected procedure [10]. The ratio between these components is the **efficiency** of the signal, which is the fraction of the desired events that is observed from the signal dataset.

$$\epsilon_S = \frac{S_f}{S_0}[10] \tag{8}$$

An algorithm was developed through C++ and ran in ROOT to access the S_f values each MC simulated signal datasets (See Appendix A). The code includes the important selection criteria of displaced vertices and momentum cuts to select the potential candidates for the process.

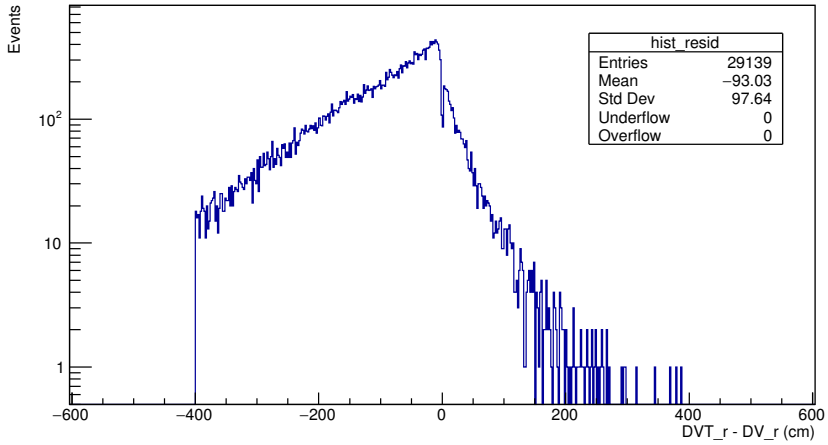

Figure 20: Residuals at $m_{Z_D} = 20$ GeV and $c\tau = 50$ cm where $S_f = 29139$ events

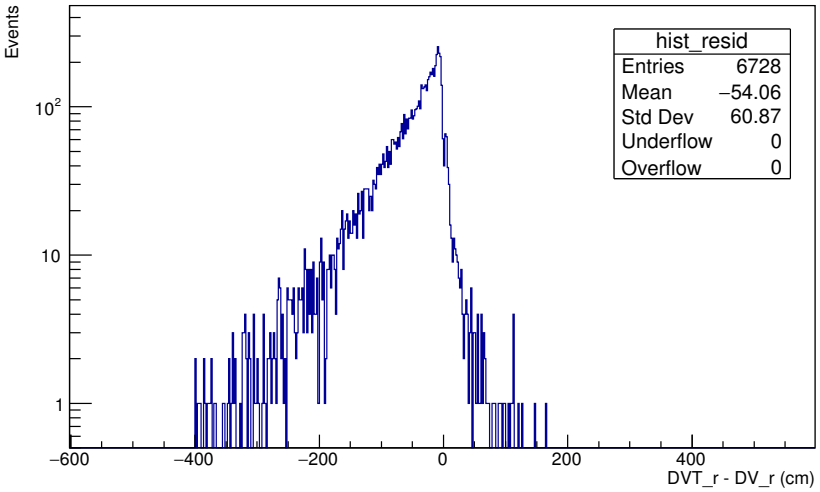

Figure 21: Residuals at $m_{Z_D} = 40$ GeV and $c\tau = 50$ cm where $S_f = 6728$ events

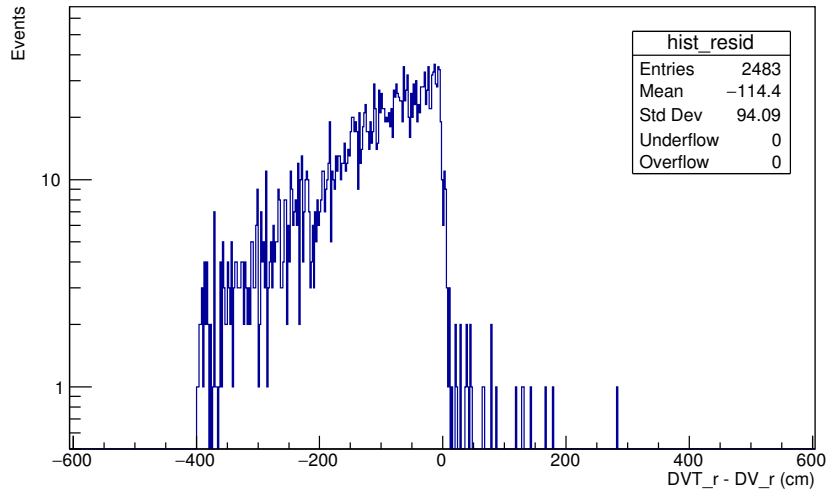

Figure 22: Residuals at $m_{Z_D} = 40$ GeV and $c\tau = 500$ cm where $S_f = 2483$ events

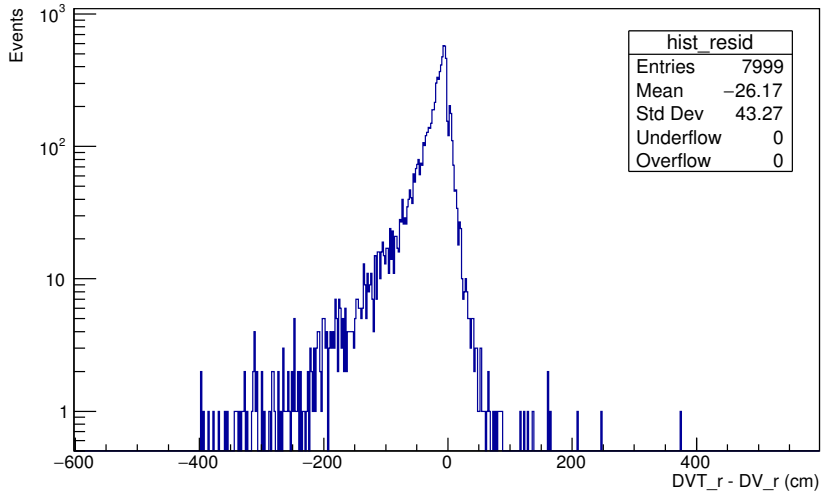

Figure 23: Residuals at $m_{Z_D} = 60$ GeV and $c\tau = 50$ cm where $S_f = 7999$ events

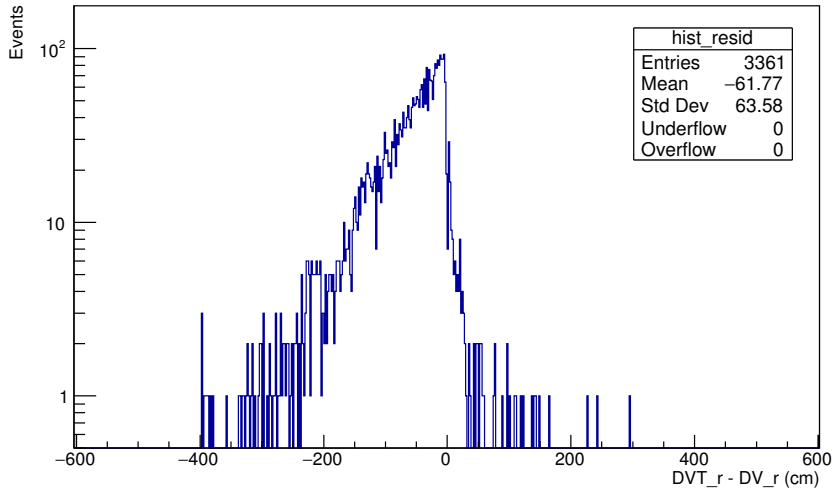

Figure 24: Residuals at $m_{Z_D} = 60$ GeV and $c\tau = 500$ cm where $S_f = 3361$ events

Figures 19-23 contains the residual between DVT_r, which contains the reconstructed ("truth") decay radius for a given Z_D that has decayed into $\mu^+\mu^-$, and DV_r, which contains the simulated decay radius. The simulation then simulates how the detectors respond to the "truth" particles. Hence, the residual shows how accurate is the reconstruction of the decay radius. The radius, r, is the distance from the IP in the xy plane. In ATLAS and other LHC experiments, cylindrical coordinates are used, hence r is the cylindrical radial coordinate. The residual is then considered the S_f value and calculating for the ratio of S_f and S_0 gives the efficiency of the signal at a certain mass and lifetime. The efficiency values for the five MC simulated datasets are summarized in the Table 3 below:

m_{Z_d}(GeV)	$c\tau$ (cm)	S_0	S_f	ϵ_S
20	50	397,999	29,139	0.0732
40	50	200,000	6,728	0.036
40	500	198,000	2,483	0.0125
60	50	200,000	7,999	0.0399
60	500	198,000	3,361	0.0169

Table 3: Efficiency values for MC simulated signal datasets

6.3 Upper Limit of Signal (N_S^{obs})

6.3.1 Poisson Processes

Poisson statistics is the appropriate model for counting experiments, where discrete counts of events are observed at a fixed rate (e.g signal and background events) [1]. The model has n events from a Poisson distribution with mean $\mu \geq 0$. These events may be either signal or background, so let $\mu_s \geq 0$ be the mean number of expected signal events in the Poisson distribution, and $\mu_b \geq 0$ be the mean number of expected background events [86]. Then $\mu = \mu_s + \mu_b$, and the probability distribution from the model becomes:

$$P(n;\mu) = \frac{e^{-\mu}\mu^n}{n!}[86] \tag{9}$$

Hence, the datasets for the exotic higgs decay mode is in a form of Poisson Distribution with background. This model would be manually created using a framework from ROOT called RooFit, which would be discussed in Chapter 6.3.5.

6.3.2 Hypothesis Testing

Analyses done mainly at the LHC, like this thesis, are concerned with the search for BSM evidence. The most common example is the searches for new particles from a signal with a known background, and detection of unpredicted decay modes from the SM. In interpreting the result of the experiment, hypothesis testing is used to make inference about the *"true physical model"*, in this case, the current Standard Model [11]. In the Poisson Model discussed in section 6.3.1, the model has assumptions defined through hypothesis testing. Before explaining these assumptions, let us define a **signal and background hypothesis ($H_{(s+b)}$)** and a **background only hypothesis (H_b)**.

Main Assumptions

$$H_0 : N_b = N_S^{obs}$$
$$H_a : N_{s+b} = N_S^{obs}$$

Since this thesis is searching for a process that does not have enough evidence yet whether it exists or not, the worst-case scenario, or the null hypothesis (H_0) is that the number of background events (N_b) is equal to the number of observed signal events in the signal dataset (N_S^{obs}). Hence, this means there is no signal and that zero events are observed. The upper limit confidence interval has to be calculated using the Poisson model applying the assumptions which are discussed in more detail in the next sections.

6.3.3 Confidence Intervals and Upper Limits

Calculating for Confidence intervals is the most common way to report errors and uncertainties on results. There are two main approaches in calculating these intervals, the **Bayesian** and **Frequentist Approaches** [65]. In the past years, there are problems encountered in the usual approaches for calculating upper confidence limits, in particular when the result is an empty set (unphysical) interval [7]. Such cases include Poisson Processes with a background. In this thesis, the main assumption for the null hypothesis is that the number of background events (N_b) is equal to the number of observed events of the signal (N_S^{obs}) for the worst case scenario,

$$N_b = N_S^{obs}$$

In the situation where zero events are observed, this case is classified as a low-signal and high-background measurement. Therefore, to calculate for upper limits of a poisson process with background, a *workspace model* in ROOT through RooFit has been created to carefully take into account the systematics of the distribution. Consequently, built-in 95% CL Upper-Limit Calculators in ROOT through RooStats were used to calculated for the 95% CL Upper-Limit of observed signals for each data set. The details of the calculations are discussed in Chapter 6.3.5.

6.3.4 Method of Calculating N_S^{obs}

ROOT is an object-oriented program and library developed by CERN for particle physics data analysis. In ROOT there are frameworks embedded that could be used for data analysis. The most important classes used in the study are **RooStats** and **RooFit**. RooStats is the common framework for statistical calculations, especially that it has built in functions that could be used to calculate for 95% CL Upper Limit of a dataset. Furthermore, the accessibility of the tools allows comparison within different statistical methods that could be used to cross-check analyzed data. On the other hand, RooFit is a framework that allows physicists

to build a *workspace model*, which could be written in any programming language. The RooFit workspace has to be created to include the uncertainties of the background from the Poisson Process. The workspace model was created using C++ and the optimistic and pessimistic scaled background events from Chapter 6.1. Using the built workspace model from RooFit, it was run through various built-in calculators in RooStats to cross-check whether different approaches agree with the calculated 95% CL Upper limit of the signal datasets. The summary of the statistical calculators used and the value of the N_S^{obs} upper-limits are shown in Tables 4 and 5 below.

Method	**95% Interval**
Profile Likelihood	$[0, 31.5532]$
Standard Bayesian	$[0.51, 36.806]$
Bayesian MCMC	$[0, 32.9149]$
Statistics Distribution	$[0, 31.5532]$
Two-Sided Frequentist	$[0, 31.25]$

Table 4: 95% CL Upper-Limit of the signal with Optimistic Background event of 127 ± 11 events with $N_S^{obs} = 32.815$ events

Method	**95% Interval**
Profile Likelihood	$[0, 250]$
Standard Feldman-Cousins	$[25, 125]$
Standard Bayesian	$[1.5365, 107.331]$
Bayesian MCMC	$[0, 95.4278]$
Two-Sided Frequentist	$[0, 143.75]$

Table 5: 95% CL Upper-Limit of the signal with Pessimistic Background event of 127 ± 45 events with $N_S^{obs} = 117.877$ events

6.4 Upper Limit of Cross Section ($\sigma^{95\%CL,UL}$) for Run 3

6.4.1 Derivation of Cross Section Equation

Cross Section is defined as:

$$\sigma = \frac{N}{\mathcal{L}} [77] \tag{10}$$

where N is the total number of events and $\mathcal{L}$ is the total integated luminosity. The cross section represents the probability that an event will occur. It is an important physical quantity because it depends on the features of the process considered but not on the specific conditions of the experiment [12]. For example, ATLAS and CMS are both general-purpose detectors of the LHC and have done similar analyses in the past. The collaborations could cross-check whether their results agree using cross-section (σ) measurements.

In the context of the LHC, two protons interact and various processes occur. In a study, a specific process of interest is within the pile of other processes. Each interesting process has an associated efficiency (ϵ_S) as discussed in Chapter 6.3, which is the percentage of all signal events reconstructed. Calculating for the cross-section becomes more complicated when it is only considering processes of interest because of the presence of background. Hence, the cross-section calculation in Equation 10 needs some modification, which is discussed in Chapter 6.4.2.

6.4.2 Calculating for $\sigma^{95\%CL,UL}$

Along with the number of observed events from the signal dataset (N_S^{obs}), efficiency (ϵ_S), and integrated luminosity for run 3 ($\int \mathcal{L}dt$), the modified cross-section upper limit at 95% CL is shown in Equation 11.

$$\sigma^{95\%CL,UL} * B = \frac{N_S^{obs}}{\epsilon_S * \int \mathcal{L}dt} [77] \tag{11}$$

N_S^{obs}: the 95% CL Upper-Limit of the signal data

ϵ_S: the efficiency of the data signal

$\int \mathcal{L}dt$: the integrated luminosity for run 3, in fb^{-1}

B: Branching ratio of the decay

$\sigma^{95\%CL,UL}$: the 95% CL Upper-Limit of the cross-section

The Tables below summarize all of the physical quantities required for the equation and the $\sigma^{95\%CL,UL}$ for run 3 using both optimistic and pessimistic approaches.

m_{Z_D}	$c\tau$	ϵ_S	N_S^{obs}	$\int \mathcal{L}dt$	$\sigma^{95\%CL,UL} * B$
20	50	0.0732	32.815	300	1.494
40	50	0.036	32.815	300	3.255
40	500	0.0125	32.815	300	8.751
60	50	0.0399	32.815	300	2.738
60	500	0.0169	32.815	300	6.472

Table 6: $\sigma^{95\%CL,UL} \times B$ with Optimistic Background event of 127 $\pm$ 11 events

m_{Z_D}	$c\tau$	ϵ_S	N_S^{obs}	$\int \mathcal{L}dt$	$\sigma^{95\%CL,UL} * B$
20	50	0.0732	117.877	300	5.367
40	50	0.036	117.877	300	11.694
40	500	0.0125	117.877	300	31.433
60	50	0.0399	117.877	300	9.835
60	500	0.0169	117.877	300	23.249

Table 7: $\sigma^{95\%CL,UL} \times B$ with Pessimistic Background event of 127 $\pm$ 45 events

6.5 Upper Limit of Cross Section ($\sigma^{95\%CL,UL}$) for Run 2

Section 6.4 explained how to calculate for the Cross Section Upper Limit for Run 3. This section shows how Run 2 Cross Section Upper Limits were obtained using plots plot from the previous analysis of the ATLAS Collaboration for this specific decay mode. This thesis would compare the cross section upper limit values of run 2 and run 3, and the plots shown in figures 25 - 27 is the upper limit cross section ($\sigma \times B$)vs cτ, which is the lifetime. Since this thesis deals with relativistic particles, the c in the lifetime is the speed of light ($3 \times 10^{10} cm/s$) and τ is the lifetime in seconds. Therefore, multiplying the two variables gives the lifetime for the relativistic particles with the units of cm. Since the lifetimes in each MC simulated dataset are known, then using the x-axis, the cross section upper limit for run 2 could be obtained in the y-axis.

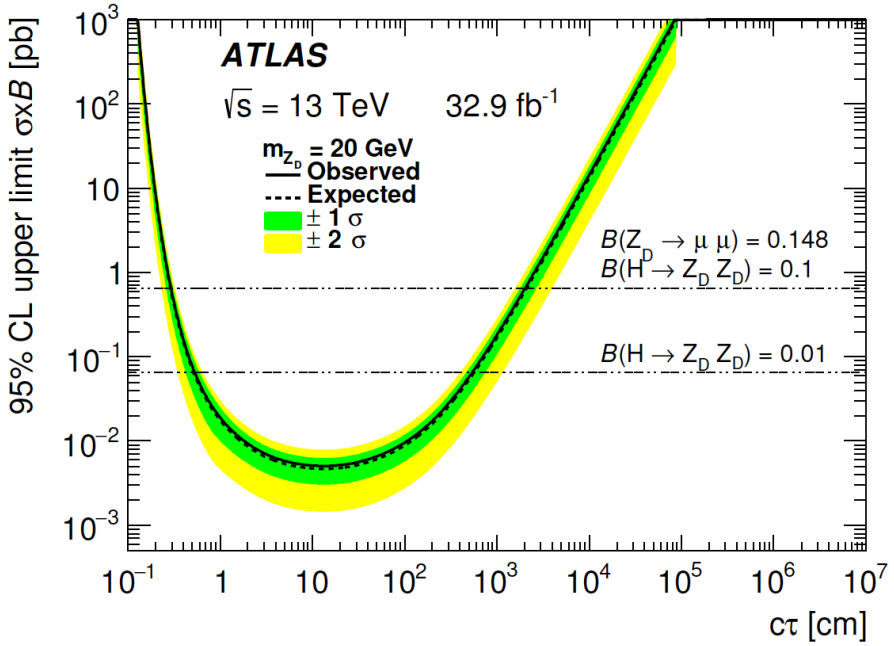

Figure 25: 95% CL UL ($\sigma \times B$) (pb) vs. range of $c\tau$ (cm) for $m_{Z_D} = 20$ GeV [28]

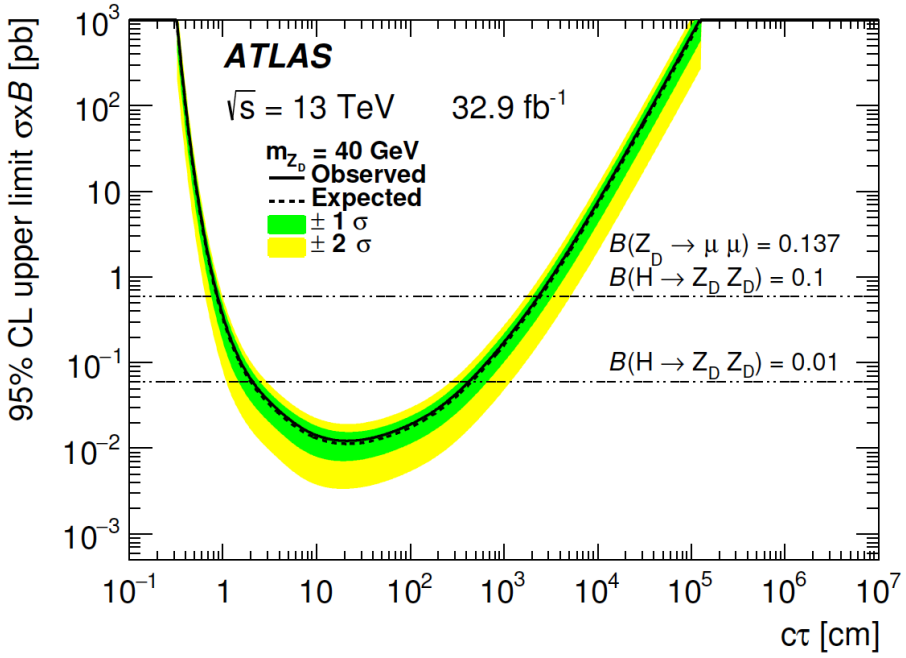

Figure 26: 95% CL UL ($\sigma \times B$) (pb) vs. range of $c\tau$ (cm) for $m_{Z_D} = 40$ GeV [28]

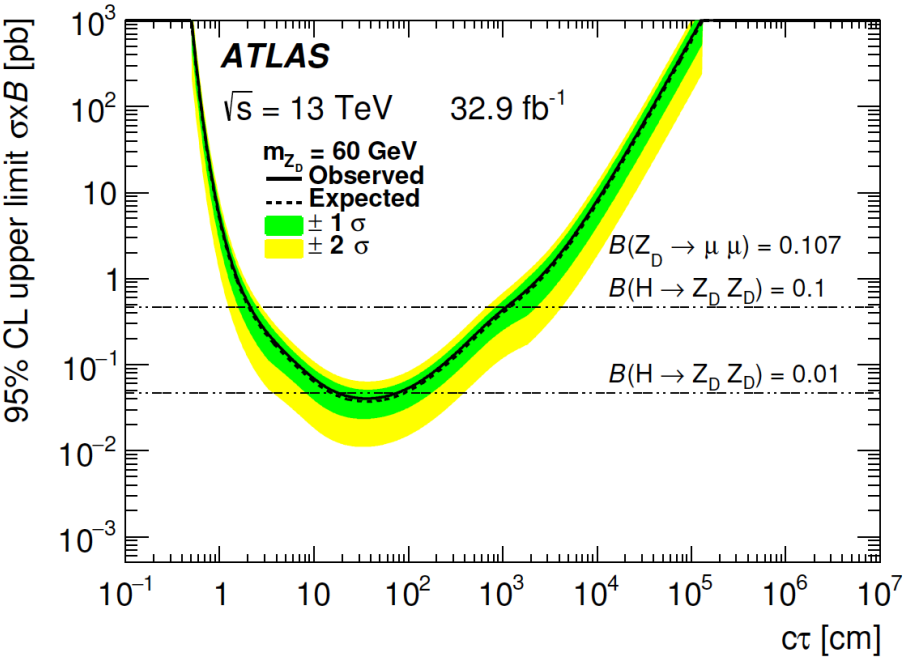

Figure 27: 95% CL UL ($\sigma \times B$) (pb) vs. range of $c\tau$ (cm) for $m_{Z_D} = 60$ GeV [28]

7 Results for the Data Samples

This chapter discusses how the 95% CL upper limit $\sigma^{95\%CL,UL}$ from the previous ATLAS study using Run 2 data differs from the calculated quantities for Run 3. The 95% CL upper limit ($\sigma \times B$) vs. $c\tau$ plots from the ATLAS paper were used to obtain the Run 2 values of the upper-limit of the cross section as shown in Figures 24 - 26. The plot presented different values of 95% CL UL $\sigma\times$B for a particular lifetime. Table 8 summarizes the mass and lifetime ranges of the Z_D, the $\sigma^{95\%CL,UL}$ for Run 2 at $\mathcal{L}_{int,Run2} = 32.9fb^{-1}$, the optimistic $\sigma^{95\%CL,UL}$ for Run 3, and the pessimistic $\sigma^{95\%CL,UL}$ for Run 3 at $\mathcal{L}_{int,Run3} = 300fb^{-1}$. A workspace model through RooFit was created to take into account the uncertainties of the background from the Poisson Process. Afterwards, 95% CL Upper-Limit Calculators were used under RooStats to calculate for the 95% CL UL of the signal of each dataset. Equation 11 in Chapter 6.4.2 was then used to convert the upper-limit of the signal to a cross-section upper limit quantity. In comparing the results From Table 8, both Run 3.1 and Run 3.2 had a smaller $\sigma^{95\%CL,UL}$ compared to Run 2. An illustration in Figure 28 explains the values in Table 8.

m_{Z_D}	$c\tau$	$\sigma^{UL}_{R2} \times B$ (fb)	$\sigma^{UL}_{R3.1} \times B$ (fb)	$\sigma^{UL}_{R3.2} \times B$ (fb)
20	50	6	1.494	5.367
40	50	15	3.255	11.694
40	500	70	8.751	31.433
60	50	45	2.738	9.835
60	500	250	6.472	23.249

Table 8: The 95% CL Upper-Limit $\sigma\times$ B for run 2 ($\sigma^{UL}_{R2} \times B$), the optimistic 95% CL Upper-Limit $\sigma\times$ B ($\sigma^{UL}_{R3.1} \times B$), and the pessimistic 95% CL Upper-Limit $\sigma\times$ B ($\sigma^{UL}_{R3.2} \times B$) for run 3 in fb for the various masses of the Z_D in GeV and their respective lifetime, $c\tau$, in cm
Using the last row an example from the table 8, the MC dataset with $m_{Z_D} = 60$

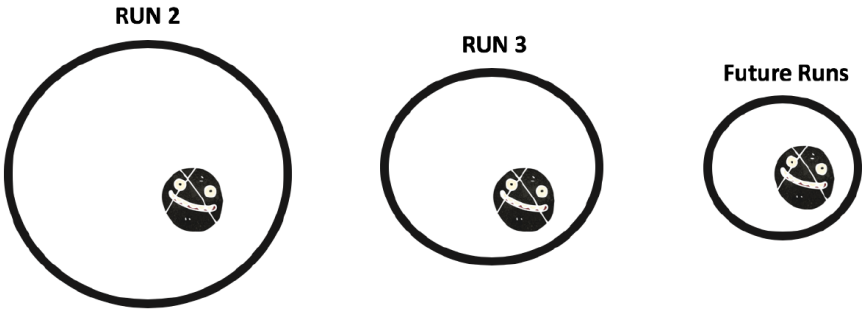

Figure 28: Illustration of a smaller $\sigma^{95\%,UL} \times B$

GeV, $c\tau = 500$ cm. For run 2, the cross section upper limit is 250 fb, the area is huge and poses a challenge to determine whether the dark photon exists within the space. As for run 3, there are two possible values given by the optimistic and

pessimistic approaches. Using the pessimistic approach with 23.249 fb, which is still 10 magnitude lower than the run 2 cross section, the cross section area is smaller. It would still be a challenge, but easier to locate this dark photon if it exists. As the detector becomes more precise and sensitive in the next few years from the upgrade, this cross section area would become smaller and smaller, that if the dark photon actually exists, physicists would eventually be able to locate the particle.

8 Summary and Next Steps

This thesis is a predictive study of the exotic higgs decay, $h \to Z_D Z_D \to 4l$ for run 3 of the ATLAS experiment with a predicted integrated luminosity of 300 fb^{-1} and center-of-mass energy of $\sqrt{s} = 14$ TeV. The extrapolation for run 3 was performed by obtaining MC Simulated datasets with Z_D mass ranges between $20 < m_{Z_D} < 60$ GeV scaled to $\mathcal{L}_{int} = 300 fb^{-1}$. Followed by using the previous run 2 background data and scaling it into $\mathcal{L}_{int} = 300 fb^{-1}$. A smaller 95% CL Upper-Limit of $\sigma \times B$ was calculated for both optimistic and pessimistic approach. This is progress because a smaller $\sigma^{95\%CL,UL}$ for run 3 could increase the chance of detecting in the signal region a significant excess in the number of displaced dimuon vertices relative to the predicted background. Next steps to take could be using the total integrated luminosity of 150 fb^{-1} of run 2 data taken from 2015 - 2018 for analysis on the $h \to Z_D Z_D \to 4l$ decay since only the 2016 run 2 data with $\mathcal{L}_{int} = 32.9 fb^{-1}$ was used. Furthermore, refining the predictive analysis done for the dark sector model and comparing it with the actual data coming from run 3 in 2021.

A Appendix

1. Efficiency Code: Applicable for all MC Simulated datasets of different Z_D mass range and lifetimes.

```
#define AnalysisEdited20GeV_11_13_cxx
#include "AnalysisEdited20GeV_11_13.h"
#include <TH2.h>
#include <TStyle.h>
#include <TCanvas.h>

using namespace std;

bool removeChambers(float eta,float phi,int numPrec) {

  //::: transition region
  if (fabs( eta ) >= 1.01 && fabs( eta ) <= 1.1 ) return false;
  //::: BIS78
  float BIS78_eta[ 2 ] = { 1.05, 1.3 };
  float BIS78_phi[ 8 ] = { 0.21, 0.57, 1.00, 1.33, 1.78, 2.14,
   2.57, 2.93 };
  if ( fabs( eta ) >= BIS78_eta[ 0 ] && fabs( eta ) <=
   BIS78_eta[ 1 ] ) {
    if ( ( fabs( phi ) >= BIS78_phi[ 0 ] && fabs( phi ) <=
   BIS78_phi[ 1 ] )
         || ( fabs( phi ) >= BIS78_phi[ 2 ] && fabs( phi ) <=
   BIS78_phi[ 3 ] )
         || ( fabs( phi ) >= BIS78_phi[ 4 ] && fabs( phi ) <=
   BIS78_phi[ 5 ] )
         || ( fabs( phi ) >= BIS78_phi[ 6 ] && fabs( phi ) <=
   BIS78_phi[ 7 ] )
        ) return false;
  }
  //::: BEE
  float BEE_eta[ 2 ] = { 1.440, 1.692 };
  float BEE_phi[ 8 ] = { 0.301, 0.478, 1.086, 1.263, 1.872,
   2.049, 2.657, 2.834 };
  if ( fabs( eta ) >= BEE_eta[ 0 ] && fabs( eta ) <= BEE_eta[ 1
    ] ) {
    if ( ( fabs( phi ) >= BEE_phi[ 0 ] && fabs( phi ) <=
   BEE_phi[ 1 ] )
         || ( fabs( phi ) >= BEE_phi[ 2 ] && fabs( phi ) <=
   BEE_phi[ 3 ] )
         || ( fabs( phi ) >= BEE_phi[ 4 ] && fabs( phi ) <=
   BEE_phi[ 5 ] )
         || ( fabs( phi ) >= BEE_phi[ 6 ] && fabs( phi ) <=
   BEE_phi[ 7 ] )
```

```
        ) {
      if (numPrec < 4) return false;
    }
  }
  return true;
}

void AnalysisEdited20GeV_11_13::Loop(TH1F* hist_resid, TH1F*
    hist_resid2)
{

  if (fChain == 0) return;

  Long64_t nentries = fChain->GetEntriesFast();

  Long64_t nbytes = 0, nb = 0;
  for (Long64_t jentry=0; jentry<nentries;jentry++) {
    Long64_t ientry = LoadTree(jentry);
    if (ientry < 0) break;
    nb = fChain->GetEntry(jentry);   nbytes += nb;
    // if (Cut(ientry) < 0) continue;
    int iMatch(-1);
    int m_debug;
    for (int j=0;j<DV_m->size();j++){

      //get lead and subleading indices
      int iL = (*DV_muIndexLead)[j];
      int iS = (*DV_muIndexSub)[j];

      //cache ntuple variables
      float DVx((*DV_x)[j]),DVy((*DV_y)[j]),DVz((*DV_z)[j]),DVr
    ((*DV_r)[j]);
      float DVl = sqrt(pow(DVr,2)+pow(DVz,2));
      //lead
      float ptL((*trk_pt)[iL]),etaL((*trk_eta)[iL]),phiL((*
    trk_phi)[iL]);
      int numPrecL = (*trk_nPrecLayers)[iL];
      //sub
      float ptS((*trk_pt)[iS]),etaS((*trk_eta)[iS]),phiS((*
    trk_phi)[iS]);
      int numPrecS = (*trk_nPrecLayers)[iS];

      //calc dRL
      int leadMatch(-1);
      float dRL(99);
      bool doIsoPlots = false;
      for (unsigned int i=0;i<comb_pt->size();i++){
```

```
74  float combPt = (*comb_pt)[i];
75  if ((*comb_isoIPV)[i] > 0.1 && !doIsoPlots) continue;  // CD:
       temporary (new v/s old Iso)
76  float JMORcut = std::min(0.04 + 10./combPt,0.4);
77  if ((*comb_JMOR)[i] < JMORcut) continue;
78  if ((*comb_author)[i] != 1) continue;
79  float dPhi = TVector2::Phi_mpi_pi((*comb_phi)[i] - phiL);
80  float dEta = (*comb_eta)[i] - etaL;
81  float dR = sqrt(pow(dPhi,2)+pow(dEta,2));
82  if (dR < dRL){
83    dRL = dR;
84    leadMatch = i;
85  }
86      }
87
88      //calc dRS
89      int subMatch(-1);
90      float dRS(99);
91      for (unsigned int i=0;i<comb_pt->size();i++){
92  float combPt = (*comb_pt)[i];
93  if ((*comb_isoIPV)[i] > 0.1 && !doIsoPlots) continue;  // CD:
       temporary (new v/s old iso)
94  float JMORcut = std::min(0.04 + 10./combPt,0.4);
95  if ((*comb_JMOR)[i] < JMORcut) continue;
96  if ((*comb_author)[i] != 1) continue;
97  float dPhi = TVector2::Phi_mpi_pi((*comb_phi)[i] - phiS);
98  float dEta = (*comb_eta)[i] - etaS;
99  float dR = sqrt(pow(dPhi,2)+pow(dEta,2));
100 if (dR < dRS){
101   dRS = dR;
102   subMatch = i;
103 }
104     }
105
106     //Preselection
107     bool passPS(true);
108
109     //calc invMass
110     bool calcInvM(true);
111     float dPhi = TVector2::Phi_mpi_pi(phiL-phiS);
112     float dEta = etaL - etaS;
113     float invM = (calcInvM) ? sqrt(2*ptL*ptS*(cosh(dEta) -
      cos(dPhi))) : (*DV_m)[j];
114
115     //Pt
116     float ptCutVal(10.0);
117     bool passPtCut = ptL > ptCutVal && ptS > ptCutVal;
```

```
118     if (!passPtCut) passPS = false;
119
120     //Precision layer requirement
121     int precLayersCut = 2;
122     bool passPrecLayers = numPrecL > precLayersCut &&
    numPrecS > precLayersCut;
123     if (!passPrecLayers) passPS = false;
124
125     //Eta layer requirement
126     int etaLayersCut = 6;
127     bool passEtaLayers = (*trk_nEtaLayers)[iL] < etaLayersCut
     && (*trk_nEtaLayers)[iS] < etaLayersCut;
128     if (!passEtaLayers) passPS = false;
129
130     //Chamber and transition removal
131     bool passPhiVeto = ((etaL < -0.33333 || etaL > 0.33333)
    || (phiL < 0.628 || phiL > 1.256)) && ((etaS < -0.33333 ||
    etaS > 0.333333) || (phiS < 0.628 || phiS > 1.256));
132     bool passChamberRemoval = removeChambers(etaL,phiL,
    numPrecL) && removeChambers(etaS,phiS,numPrecS) &&
    passPhiVeto;
133     if (!passChamberRemoval) passPS = false;
134
135     //d0 sigma
136     float maxD0Sig = 20.;
137     bool passD0Sig = sqrt((*trk_covd0)[iL]) < maxD0Sig &&
    sqrt((*trk_covd0)[iS]) < maxD0Sig;
138     if (!passD0Sig) passPS = false;
139
140     //fiducialVol;
141     float maxEta(2.4);
142     float maxZ(600.);
143     float maxR(400.);
144     bool passFidVol = TMath::Abs(etaL) < maxEta && TMath::Abs
    (etaS) < maxEta && TMath::Abs(DVz) < maxZ && TMath::Abs(DVr)
     < maxR;
145     if (!passFidVol) passPS = false;
146
147     //trkDist
148     float minTrkDist(0.0);
149     float maxTrkDist(20.0);
150     float trkDist = (*DV_distV)[j];
151     bool passTrkDist = trkDist < maxTrkDist && trkDist >
    minTrkDist;
152     if (!passTrkDist) passPS = false;
153
154     //trkAng
```

```
155         double minTrkAng(0.1);
156         bool passTrkAng = (*DV_openAng)[j] > minTrkAng;
157         if (!passTrkAng) passPS = false;
158 
159         //InvMass
160         float minInvMass(15.);
161         float maxInvMass(70.);
162         bool passInvMass = invM > minInvMass && invM < maxInvMass
    ;
163         if (!passInvMass) passPS = false;
164 
165         //QCD Vars
166 
167         //MaxIso
168         double IsoCut = 0.05;
169         double isoL = (*trk_isoIPV)[iL];
170         double isoS = (*trk_isoIPV)[iS];
171         double minIso = std::min(isoL,isoS);
172         double maxIso = std::max(isoL,isoS);
173         bool passIso = maxIso < IsoCut;
174 
175         //JMOR
176         float JMORcutL = std::min(0.04 + 10./ptL,0.4);
177         float JMORcutS = std::min(0.04 + 10./ptS,0.4);
178         bool passJMOR = (*trk_jetDR)[iL] > JMORcutL && (*
    trk_jetDR)[iS] > JMORcutS;
179 
180         //Charge
181         float qVtx = (*DV_charge)[j];
182         bool OSVtx = (qVtx == 0.); // CD:  toggle to do OS v/s SS
183 
184         //Cosmic
185         double deltaPhi = fabs(TVector2::Phi_mpi_pi(phiL - phiS))
    ;
186         double sumEta = fabs(etaL + etaS);
187         double drCos = sqrt(pow(sumEta,2) + pow(TMath::Pi() -
    deltaPhi,2));
188         bool passCosmic = drCos > 0.1;
189 
190         //Signal region:  minDRReq = 0.1, maxDRReq = 10 (any
    number larger than 5 works)
191 
192         bool passSR = passPS && passCosmic && passIso && passJMOR
     && OSVtx; //pass preselection/nominal
193 
194         if (passSR == true){
195     hist_resid2->Fill((*DVT_l)[iMatch] - (*DV_l)[j]);
```

```
196     hist_resid->Fill((*DVT_r)[iMatch] - (*DV_r)[j]);
197         }
198       }
199     }
200 }
201 
202 int run(){
203   AnalysisEdited20GeV_11_13 m;
204   TH1F* hist_resid = new TH1F("hist_resid", " ", 1000, -1000,
        1000); //Residual Plot of Displaced Vertices for 20 GeV
205   //TH1F* hist_resid = new TH1F("hist_resid", "Residual Plot
        with Truth Matching of DVT_r and DV_r", 10000, 290000,
        30000);  // 10, -50, 50
206   TH1F* hist_resid2 = new TH1F("hist_resid2", "Residual Plot
        with Truth Matching of DVT_l and DV_l", 10000, -5000, 5000);
          // 10, -50, 50
207 
208   m.Loop(hist_resid, hist_resid2);
209 
210   //TFile f("Residuals20_1113.root", "Recreate");
211   TFile f("Residuals20GeV_230419.root", "Recreate");
212   f.cd();
213   gStyle->SetOptStat(111111);
214 
215   hist_resid->GetXaxis()->SetTitle("DVT_r - DV_r");
216   hist_resid->GetYaxis()->SetTitle("Events");
217   hist_resid->Write();
218 
219   hist_resid2->GetXaxis()->SetTitle("");
220   hist_resid2->GetYaxis()->SetTitle("");
221   hist_resid2->Write();
222 
223   delete hist_resid;
224   delete hist_resid2;
225 
226   return 0;
227 }
```

2. Header File accompanying the Efficiency Code.

```
//////////////////////////////////////////////////////////
// This class has been automatically generated on
// Tue Nov 13 14:50:16 2018 by ROOT version 6.12/04
// from TTree tree/tree
// found on file: Tree.root
//////////////////////////////////////////////////////////

#ifndef AnalysisEdited20GeV_11_13_h
#define AnalysisEdited20GeV_11_13_h

#include <TROOT.h>
#include <TChain.h>
#include <TFile.h>

// Header file for the classes stored in the TTree if any.
#include "vector"
#include "vector"
#include "vector"
#include "vector"

class AnalysisEdited20GeV_11_13 {
public :
   TTree          *fChain;   //!pointer to the analyzed TTree or TChain
   Int_t           fCurrent; //!current Tree number in a TChain

// Fixed size dimensions of array or collections stored in the TTree if any.

   // Declaration of leaf types
   Int_t           EventNumber;
   Int_t           RunNumber;
   Int_t           BCID;
   Int_t           LB;
   Float_t         evtWeight;
   Float_t         sumWeights;
   Float_t         prw;
   Float_t         EtMiss;
   Float_t         EtMissPhi;
   Float_t         TPV_x;
   Float_t         TPV_y;
   Float_t         TPV_z;
   Float_t         PV_z;
   Int_t           PV_ntrk;
   Int_t           PU_nvtx;
   Int_t           nMSOnly;
```

```
45    Int_t           NDV;
46    Int_t           NDVT;
47    Int_t           narrowScanTrig;
48    Int_t           METTrig;
49    Int_t           singleMuTrig;
50    Int_t           threeMuTrig;
51    Int_t           L1_MU20Trig;
52    Int_t           L1_3MU6Trig;
53    Float_t         trigMHT;
54    Float_t         trigMHTPhi;
55    Float_t         MHT;
56    Float_t         MHTPhi;
57    vector<float>   *id_pt;
58    vector<float>   *id_phi;
59    vector<float>   *id_eta;
60    vector<float>   *id_d0;
61    vector<float>   *id_z0;
62    vector<float>   *id_charge;
63    vector<float>   *id_chi2;
64    vector<float>   *id_dof;
65    vector<int>     *id_vtxType;
66    vector<float>   *trkt_pt;
67    vector<float>   *trkt_phi;
68    vector<float>   *trkt_eta;
69    vector<float>   *trkt_d0;
70    vector<float>   *trkt_z0;
71    vector<float>   *trkt_charge;
72    vector<int>     *trkt_PDG;
73    vector<int>     *trkt_barCode;
74    vector<int>     *trkt_status;
75    vector<int>     *trkt_parPDG;
76    vector<int>     *trkt_parBarCode;
77    vector<int>     *DVT_LJMatch;
78    vector<int>     *DVT_mu60Match;
79    vector<float>   *DVT_x;
80    vector<float>   *DVT_y;
81    vector<float>   *DVT_z;
82    vector<float>   *DVT_r;
83    vector<float>   *DVT_l;
84    vector<float>   *DVT_m;
85    vector<float>   *DVT_openAng;
86    vector<int>     *DVT_parPDG;
87    vector<int>     *DVT_parBarCode;
88    vector<int>     *DVT_muIndexLead;
89    vector<int>     *DVT_muIndexSub;
90    vector<double>  *DVT_pLLP;
91    vector<double>  *DVT_eLLP;
```

```
92    vector<double>  *DVT_lLLP;
93    vector<float>   *comb_pt;
94    vector<float>   *comb_phi;
95    vector<float>   *comb_eta;
96    vector<float>   *comb_d0;
97    vector<float>   *comb_z0;
98    vector<float>   *comb_isoDPV;
99    vector<float>   *comb_isoDAll;
100   vector<float>   *comb_isoIPV;
101   vector<float>   *comb_isoIAll;
102   vector<float>   *comb_JMOR;
103   vector<int>     *comb_author;
104   vector<double>  *comb_chi2;
105   vector<int>     *comb_PDG;
106   vector<int>     *comb_barcode;
107   vector<float>   *trk_pt;
108   vector<float>   *trk_phi;
109   vector<float>   *trk_eta;
110   vector<float>   *trk_d0;
111   vector<float>   *trk_z0;
112   vector<float>   *trk_m;
113   vector<float>   *trk_charge;
114   vector<float>   *trk_covd0;
115   vector<float>   *trk_covz0;
116   vector<float>   *trk_covPhi;
117   vector<float>   *trk_covTheta;
118   vector<float>   *trk_covP;
119   Int_t           trk_isTM;
120   vector<int>     *trk_PDG;
121   vector<int>     *trk_barCode;
122   vector<int>     *trk_parPDG;
123   vector<int>     *trk_parBarCode;
124   vector<float>   *trk_isoDPV;
125   vector<float>   *trk_isoDAll;
126   vector<float>   *trk_isoIPV;
127   vector<float>   *trk_isoIAll;
128   vector<float>   *trk_jetDR;
129   vector<unsigned char> *trk_nPrecLayers;
130   vector<unsigned char> *trk_nPhiLayers;
131   vector<unsigned char> *trk_nEtaLayers;
132   vector<float>   *trk_vx;
133   vector<float>   *trk_vy;
134   vector<float>   *trk_vz;
135   vector<float>   *DV_x;
136   vector<float>   *DV_y;
137   vector<float>   *DV_z;
138   vector<float>   *DV_r;
```

```
139     vector<float>   *DV_l;
140     vector<float>   *DV_m;
141     vector<float>   *DV_charge;
142     vector<float>   *DV_openAng;
143     vector<float>   *DV_distV;
144     vector<int>     *DV_muIndexLead;
145     vector<int>     *DV_muIndexSub;
146 
147     // List of branches
148     TBranch         *b_EventNumber;    //!
149     TBranch         *b_RunNumber;    //!
150     TBranch         *b_BCID;    //!
151     TBranch         *b_LB;    //!
152     TBranch         *b_evtWeight;    //!
153     TBranch         *b_sumWeights;    //!
154     TBranch         *b_prw;    //!
155     TBranch         *b_EtMiss;    //!
156     TBranch         *b_EtMissPhi;    //!
157     TBranch         *b_TPV_x;    //!
158     TBranch         *b_TPV_y;    //!
159     TBranch         *b_TPV_z;    //!
160     TBranch         *b_PV_z;    //!
161     TBranch         *b_PV_ntrk;    //!
162     TBranch         *b_PU_nvtx;    //!
163     TBranch         *b_nMSOnly;    //!
164     TBranch         *b_NDV;    //!
165     TBranch         *b_NDVT;    //!
166     TBranch         *b_narrowScanTrig;    //!
167     TBranch         *b_METTrig;    //!
168     TBranch         *b_singleMuTrig;    //!
169     TBranch         *b_threeMuTrig;    //!
170     TBranch         *b_L1_MU20Trig;    //!
171     TBranch         *b_L1_3MU6Trig;    //!
172     TBranch         *b_trigMHT;    //!
173     TBranch         *b_trigMHTPhi;    //!
174     TBranch         *b_MHT;    //!
175     TBranch         *b_MHTPhi;    //!
176     TBranch         *b_id_pt;    //!
177     TBranch         *b_id_phi;    //!
178     TBranch         *b_id_eta;    //!
179     TBranch         *b_id_d0;    //!
180     TBranch         *b_id_z0;    //!
181     TBranch         *b_id_charge;    //!
182     TBranch         *b_id_chi2;    //!
183     TBranch         *b_id_dof;    //!
184     TBranch         *b_id_vtxType;    //!
185     TBranch         *b_trkt_pt;    //!
```

```
186     TBranch        *b_trkt_phi;    //!
187     TBranch        *b_trkt_eta;    //!
188     TBranch        *b_trkt_d0;    //!
189     TBranch        *b_trkt_z0;    //!
190     TBranch        *b_trkt_charge;    //!
191     TBranch        *b_trkt_PDG;    //!
192     TBranch        *b_trkt_barCode;    //!
193     TBranch        *b_trkt_status;    //!
194     TBranch        *b_trkt_parPDG;    //!
195     TBranch        *b_trkt_parBarCode;    //!
196     TBranch        *b_DVT_LJMatch;    //!
197     TBranch        *b_DVT_mu60Match;    //!
198     TBranch        *b_DVT_x;    //!
199     TBranch        *b_DVT_y;    //!
200     TBranch        *b_DVT_z;    //!
201     TBranch        *b_DVT_r;    //!
202     TBranch        *b_DVT_l;    //!
203     TBranch        *b_DVT_m;    //!
204     TBranch        *b_DVT_openAng;    //!
205     TBranch        *b_DVT_parPDG;    //!
206     TBranch        *b_DVT_parBarCode;    //!
207     TBranch        *b_DVT_muIndexLead;    //!
208     TBranch        *b_DVT_muIndexSub;    //!
209     TBranch        *b_DVT_pLLP;    //!
210     TBranch        *b_DVT_eLLP;    //!
211     TBranch        *b_DVT_lLLP;    //!
212     TBranch        *b_comb_pt;    //!
213     TBranch        *b_comb_phi;    //!
214     TBranch        *b_comb_eta;    //!
215     TBranch        *b_comb_d0;    //!
216     TBranch        *b_comb_z0;    //!
217     TBranch        *b_comb_isoDPV;    //!
218     TBranch        *b_comb_isoDAll;    //!
219     TBranch        *b_comb_isoIPV;    //!
220     TBranch        *b_comb_isoIAll;    //!
221     TBranch        *b_comb_JMOR;    //!
222     TBranch        *b_comb_author;    //!
223     TBranch        *b_comb_chi2;    //!
224     TBranch        *b_comb_PDG;    //!
225     TBranch        *b_comb_barcode;    //!
226     TBranch        *b_trk_pt;    //!
227     TBranch        *b_trk_phi;    //!
228     TBranch        *b_trk_eta;    //!
229     TBranch        *b_trk_d0;    //!
230     TBranch        *b_trk_z0;    //!
231     TBranch        *b_trk_m;    //!
232     TBranch        *b_trk_charge;    //!
```

```
233    TBranch        *b_trk_covd0;   //!
234    TBranch        *b_trk_covz0;   //!
235    TBranch        *b_trk_covPhi;   //!
236    TBranch        *b_trk_covTheta;   //!
237    TBranch        *b_trk_covP;   //!
238    TBranch        *b_trk_isTM;   //!
239    TBranch        *b_trk_PDG;   //!
240    TBranch        *b_trk_barCode;   //!
241    TBranch        *b_trk_parPDG;   //!
242    TBranch        *b_trk_parBarCode;   //!
243    TBranch        *b_trk_isoDPV;   //!
244    TBranch        *b_trk_isoDAll;   //!
245    TBranch        *b_trk_isoIPV;   //!
246    TBranch        *b_trk_isoIAll;   //!
247    TBranch        *b_trk_jetDR;   //!
248    TBranch        *b_trk_nPrecLayers;   //!
249    TBranch        *b_trk_nPhiLayers;   //!
250    TBranch        *b_trk_nEtaLayers;   //!
251    TBranch        *b_trk_vx;   //!
252    TBranch        *b_trk_vy;   //!
253    TBranch        *b_trk_vz;   //!
254    TBranch        *b_DV_x;   //!
255    TBranch        *b_DV_y;   //!
256    TBranch        *b_DV_z;   //!
257    TBranch        *b_DV_r;   //!
258    TBranch        *b_DV_l;   //!
259    TBranch        *b_DV_m;   //!
260    TBranch        *b_DV_charge;   //!
261    TBranch        *b_DV_openAng;   //!
262    TBranch        *b_DV_distV;   //!
263    TBranch        *b_DV_muIndexLead;   //!
264    TBranch        *b_DV_muIndexSub;   //!
265
266    AnalysisEdited20GeV_11_13(TTree *tree=0);
267    virtual ~AnalysisEdited20GeV_11_13();
268    virtual Int_t    Cut(Long64_t entry);
269    virtual Int_t    GetEntry(Long64_t entry);
270    virtual Long64_t LoadTree(Long64_t entry);
271    virtual void     Init(TTree *tree);
272    virtual void     Loop(TH1F* hist_resid, TH1F* hist_resid2);
273    virtual Bool_t   Notify();
274    virtual void     Show(Long64_t entry = -1);
275 };
276
277 #endif
278
279 #ifdef AnalysisEdited20GeV_11_13_cxx
```

```
280 AnalysisEdited20GeV_11_13::AnalysisEdited20GeV_11_13(TTree *
    tree) : fChain(0)
281 {
282 // if parameter tree is not specified (or zero), connect the
    file
283 // used to generate this class and read the Tree.
284    if (tree == 0) {
285       TFile *f = (TFile*)gROOT->GetListOfFiles()->FindObject("
    Tree.root");
286       if (!f || !f->IsOpen()) {
287          f = new TFile("Tree.root");
288       }
289       f->GetObject("tree",tree);
290
291    }
292    Init(tree);
293 }
294
295 AnalysisEdited20GeV_11_13::~AnalysisEdited20GeV_11_13()
296 {
297    if (!fChain) return;
298    delete fChain->GetCurrentFile();
299 }
300
301 Int_t AnalysisEdited20GeV_11_13::GetEntry(Long64_t entry)
302 {
303 // Read contents of entry.
304    if (!fChain) return 0;
305    return fChain->GetEntry(entry);
306 }
307 Long64_t AnalysisEdited20GeV_11_13::LoadTree(Long64_t entry)
308 {
309 // Set the environment to read one entry
310    if (!fChain) return -5;
311    Long64_t centry = fChain->LoadTree(entry);
312    if (centry < 0) return centry;
313    if (fChain->GetTreeNumber() != fCurrent) {
314       fCurrent = fChain->GetTreeNumber();
315       Notify();
316    }
317    return centry;
318 }
319
320 void AnalysisEdited20GeV_11_13::Init(TTree *tree)
321 {
322    // The Init() function is called when the selector needs to
    initialize
```

```
323     // a new tree or chain. Typically here the branch addresses
        and branch
324     // pointers of the tree will be set.
325     // It is normally not necessary to make changes to the
        generated
326     // code, but the routine can be extended by the user if
        needed.
327     // Init() will be called many times when running on PROOF
328     // (once per file to be processed).
329
330     // Set object pointer
331     id_pt = 0;
332     id_phi = 0;
333     id_eta = 0;
334     id_d0 = 0;
335     id_z0 = 0;
336     id_charge = 0;
337     id_chi2 = 0;
338     id_dof = 0;
339     id_vtxType = 0;
340     trkt_pt = 0;
341     trkt_phi = 0;
342     trkt_eta = 0;
343     trkt_d0 = 0;
344     trkt_z0 = 0;
345     trkt_charge = 0;
346     trkt_PDG = 0;
347     trkt_barCode = 0;
348     trkt_status = 0;
349     trkt_parPDG = 0;
350     trkt_parBarCode = 0;
351     DVT_LJMatch = 0;
352     DVT_mu60Match = 0;
353     DVT_x = 0;
354     DVT_y = 0;
355     DVT_z = 0;
356     DVT_r = 0;
357     DVT_l = 0;
358     DVT_m = 0;
359     DVT_openAng = 0;
360     DVT_parPDG = 0;
361     DVT_parBarCode = 0;
362     DVT_muIndexLead = 0;
363     DVT_muIndexSub = 0;
364     DVT_pLLP = 0;
365     DVT_eLLP = 0;
366     DVT_lLLP = 0;
```

```
367     comb_pt = 0;
368     comb_phi = 0;
369     comb_eta = 0;
370     comb_d0 = 0;
371     comb_z0 = 0;
372     comb_isoDPV = 0;
373     comb_isoDAll = 0;
374     comb_isoIPV = 0;
375     comb_isoIAll = 0;
376     comb_JMOR = 0;
377     comb_author = 0;
378     comb_chi2 = 0;
379     comb_PDG = 0;
380     comb_barcode = 0;
381     trk_pt = 0;
382     trk_phi = 0;
383     trk_eta = 0;
384     trk_d0 = 0;
385     trk_z0 = 0;
386     trk_m = 0;
387     trk_charge = 0;
388     trk_covd0 = 0;
389     trk_covz0 = 0;
390     trk_covPhi = 0;
391     trk_covTheta = 0;
392     trk_covP = 0;
393     trk_PDG = 0;
394     trk_barCode = 0;
395     trk_parPDG = 0;
396     trk_parBarCode = 0;
397     trk_isoDPV = 0;
398     trk_isoDAll = 0;
399     trk_isoIPV = 0;
400     trk_isoIAll = 0;
401     trk_jetDR = 0;
402     trk_nPrecLayers = 0;
403     trk_nPhiLayers = 0;
404     trk_nEtaLayers = 0;
405     trk_vx = 0;
406     trk_vy = 0;
407     trk_vz = 0;
408     DV_x = 0;
409     DV_y = 0;
410     DV_z = 0;
411     DV_r = 0;
412     DV_l = 0;
413     DV_m = 0;
```

```
414     DV_charge = 0;
415     DV_openAng = 0;
416     DV_distV = 0;
417     DV_muIndexLead = 0;
418     DV_muIndexSub = 0;
419     // Set branch addresses and branch pointers
420     if (!tree) return;
421     fChain = tree;
422     fCurrent = -1;
423     fChain->SetMakeClass(1);
424
425     fChain->SetBranchAddress("EventNumber", &EventNumber, &
        b_EventNumber);
426     fChain->SetBranchAddress("RunNumber", &RunNumber, &
        b_RunNumber);
427     fChain->SetBranchAddress("BCID", &BCID, &b_BCID);
428     fChain->SetBranchAddress("LB", &LB, &b_LB);
429     fChain->SetBranchAddress("evtWeight", &evtWeight, &
        b_evtWeight);
430     fChain->SetBranchAddress("sumWeights", &sumWeights, &
        b_sumWeights);
431     fChain->SetBranchAddress("prw", &prw, &b_prw);
432     fChain->SetBranchAddress("EtMiss", &EtMiss, &b_EtMiss);
433     fChain->SetBranchAddress("EtMissPhi", &EtMissPhi, &
        b_EtMissPhi);
434     fChain->SetBranchAddress("TPV_x", &TPV_x, &b_TPV_x);
435     fChain->SetBranchAddress("TPV_y", &TPV_y, &b_TPV_y);
436     fChain->SetBranchAddress("TPV_z", &TPV_z, &b_TPV_z);
437     fChain->SetBranchAddress("PV_z", &PV_z, &b_PV_z);
438     fChain->SetBranchAddress("PV_ntrk", &PV_ntrk, &b_PV_ntrk);
439     fChain->SetBranchAddress("PU_nvtx", &PU_nvtx, &b_PU_nvtx);
440     fChain->SetBranchAddress("nMSOnly", &nMSOnly, &b_nMSOnly);
441     fChain->SetBranchAddress("NDV", &NDV, &b_NDV);
442     fChain->SetBranchAddress("NDVT", &NDVT, &b_NDVT);
443     fChain->SetBranchAddress("narrowScanTrig", &narrowScanTrig,
        &b_narrowScanTrig);
444     fChain->SetBranchAddress("METTrig", &METTrig, &b_METTrig);
445     fChain->SetBranchAddress("singleMuTrig", &singleMuTrig, &
        b_singleMuTrig);
446     fChain->SetBranchAddress("threeMuTrig", &threeMuTrig, &
        b_threeMuTrig);
447     fChain->SetBranchAddress("L1_MU20Trig", &L1_MU20Trig, &
        b_L1_MU20Trig);
448     fChain->SetBranchAddress("L1_3MU6Trig", &L1_3MU6Trig, &
        b_L1_3MU6Trig);
449     fChain->SetBranchAddress("trigMHT", &trigMHT, &b_trigMHT);
450     fChain->SetBranchAddress("trigMHTPhi", &trigMHTPhi, &
```

```
    b_trigMHTPhi);
451 fChain->SetBranchAddress("MHT", &MHT, &b_MHT);
452 fChain->SetBranchAddress("MHTPhi", &MHTPhi, &b_MHTPhi);
453 fChain->SetBranchAddress("id_pt", &id_pt, &b_id_pt);
454 fChain->SetBranchAddress("id_phi", &id_phi, &b_id_phi);
455 fChain->SetBranchAddress("id_eta", &id_eta, &b_id_eta);
456 fChain->SetBranchAddress("id_d0", &id_d0, &b_id_d0);
457 fChain->SetBranchAddress("id_z0", &id_z0, &b_id_z0);
458 fChain->SetBranchAddress("id_charge", &id_charge, &
    b_id_charge);
459 fChain->SetBranchAddress("id_chi2", &id_chi2, &b_id_chi2);
460 fChain->SetBranchAddress("id_dof", &id_dof, &b_id_dof);
461 fChain->SetBranchAddress("id_vtxType", &id_vtxType, &
    b_id_vtxType);
462 fChain->SetBranchAddress("trkt_pt", &trkt_pt, &b_trkt_pt);
463 fChain->SetBranchAddress("trkt_phi", &trkt_phi, &b_trkt_phi)
    ;
464 fChain->SetBranchAddress("trkt_eta", &trkt_eta, &b_trkt_eta)
    ;
465 fChain->SetBranchAddress("trkt_d0", &trkt_d0, &b_trkt_d0);
466 fChain->SetBranchAddress("trkt_z0", &trkt_z0, &b_trkt_z0);
467 fChain->SetBranchAddress("trkt_charge", &trkt_charge, &
    b_trkt_charge);
468 fChain->SetBranchAddress("trkt_PDG", &trkt_PDG, &b_trkt_PDG)
    ;
469 fChain->SetBranchAddress("trkt_barCode", &trkt_barCode, &
    b_trkt_barCode);
470 fChain->SetBranchAddress("trkt_status", &trkt_status, &
    b_trkt_status);
471 fChain->SetBranchAddress("trkt_parPDG", &trkt_parPDG, &
    b_trkt_parPDG);
472 fChain->SetBranchAddress("trkt_parBarCode", &trkt_parBarCode
    , &b_trkt_parBarCode);
473 fChain->SetBranchAddress("DVT_LJMatch", &DVT_LJMatch, &
    b_DVT_LJMatch);
474 fChain->SetBranchAddress("DVT_mu60Match", &DVT_mu60Match, &
    b_DVT_mu60Match);
475 fChain->SetBranchAddress("DVT_x", &DVT_x, &b_DVT_x);
476 fChain->SetBranchAddress("DVT_y", &DVT_y, &b_DVT_y);
477 fChain->SetBranchAddress("DVT_z", &DVT_z, &b_DVT_z);
478 fChain->SetBranchAddress("DVT_r", &DVT_r, &b_DVT_r);
479 fChain->SetBranchAddress("DVT_l", &DVT_l, &b_DVT_l);
480 fChain->SetBranchAddress("DVT_m", &DVT_m, &b_DVT_m);
481 fChain->SetBranchAddress("DVT_openAng", &DVT_openAng, &
    b_DVT_openAng);
482 fChain->SetBranchAddress("DVT_parPDG", &DVT_parPDG, &
    b_DVT_parPDG);
```

```
483     fChain->SetBranchAddress("DVT_parBarCode", &DVT_parBarCode,
        &b_DVT_parBarCode);
484     fChain->SetBranchAddress("DVT_muIndexLead", &DVT_muIndexLead
        , &b_DVT_muIndexLead);
485     fChain->SetBranchAddress("DVT_muIndexSub", &DVT_muIndexSub,
        &b_DVT_muIndexSub);
486     fChain->SetBranchAddress("DVT_pLLP", &DVT_pLLP, &b_DVT_pLLP)
        ;
487     fChain->SetBranchAddress("DVT_eLLP", &DVT_eLLP, &b_DVT_eLLP)
        ;
488     fChain->SetBranchAddress("DVT_lLLP", &DVT_lLLP, &b_DVT_lLLP)
        ;
489     fChain->SetBranchAddress("comb_pt", &comb_pt, &b_comb_pt);
490     fChain->SetBranchAddress("comb_phi", &comb_phi, &b_comb_phi)
        ;
491     fChain->SetBranchAddress("comb_eta", &comb_eta, &b_comb_eta)
        ;
492     fChain->SetBranchAddress("comb_d0", &comb_d0, &b_comb_d0);
493     fChain->SetBranchAddress("comb_z0", &comb_z0, &b_comb_z0);
494     fChain->SetBranchAddress("comb_isoDPV", &comb_isoDPV, &
        b_comb_isoDPV);
495     fChain->SetBranchAddress("comb_isoDAll", &comb_isoDAll, &
        b_comb_isoDAll);
496     fChain->SetBranchAddress("comb_isoIPV", &comb_isoIPV, &
        b_comb_isoIPV);
497     fChain->SetBranchAddress("comb_isoIAll", &comb_isoIAll, &
        b_comb_isoIAll);
498     fChain->SetBranchAddress("comb_JMOR", &comb_JMOR, &
        b_comb_JMOR);
499     fChain->SetBranchAddress("comb_author", &comb_author, &
        b_comb_author);
500     fChain->SetBranchAddress("comb_chi2", &comb_chi2, &
        b_comb_chi2);
501     fChain->SetBranchAddress("comb_PDG", &comb_PDG, &b_comb_PDG)
        ;
502     fChain->SetBranchAddress("comb_barcode", &comb_barcode, &
        b_comb_barcode);
503     fChain->SetBranchAddress("trk_pt", &trk_pt, &b_trk_pt);
504     fChain->SetBranchAddress("trk_phi", &trk_phi, &b_trk_phi);
505     fChain->SetBranchAddress("trk_eta", &trk_eta, &b_trk_eta);
506     fChain->SetBranchAddress("trk_d0", &trk_d0, &b_trk_d0);
507     fChain->SetBranchAddress("trk_z0", &trk_z0, &b_trk_z0);
508     fChain->SetBranchAddress("trk_m", &trk_m, &b_trk_m);
509     fChain->SetBranchAddress("trk_charge", &trk_charge, &
        b_trk_charge);
510     fChain->SetBranchAddress("trk_covd0", &trk_covd0, &
        b_trk_covd0);
```

```
511     fChain->SetBranchAddress("trk_covz0", &trk_covz0, &
        b_trk_covz0);
512     fChain->SetBranchAddress("trk_covPhi", &trk_covPhi, &
        b_trk_covPhi);
513     fChain->SetBranchAddress("trk_covTheta", &trk_covTheta, &
        b_trk_covTheta);
514     fChain->SetBranchAddress("trk_covP", &trk_covP, &b_trk_covP)
        ;
515     fChain->SetBranchAddress("trk_isTM", &trk_isTM, &b_trk_isTM)
        ;
516     fChain->SetBranchAddress("trk_PDG", &trk_PDG, &b_trk_PDG);
517     fChain->SetBranchAddress("trk_barCode", &trk_barCode, &
        b_trk_barCode);
518     fChain->SetBranchAddress("trk_parPDG", &trk_parPDG, &
        b_trk_parPDG);
519     fChain->SetBranchAddress("trk_parBarCode", &trk_parBarCode,
        &b_trk_parBarCode);
520     fChain->SetBranchAddress("trk_isoDPV", &trk_isoDPV, &
        b_trk_isoDPV);
521     fChain->SetBranchAddress("trk_isoDAll", &trk_isoDAll, &
        b_trk_isoDAll);
522     fChain->SetBranchAddress("trk_isoIPV", &trk_isoIPV, &
        b_trk_isoIPV);
523     fChain->SetBranchAddress("trk_isoIAll", &trk_isoIAll, &
        b_trk_isoIAll);
524     fChain->SetBranchAddress("trk_jetDR", &trk_jetDR, &
        b_trk_jetDR);
525     fChain->SetBranchAddress("trk_nPrecLayers", &trk_nPrecLayers
        , &b_trk_nPrecLayers);
526     fChain->SetBranchAddress("trk_nPhiLayers", &trk_nPhiLayers,
        &b_trk_nPhiLayers);
527     fChain->SetBranchAddress("trk_nEtaLayers", &trk_nEtaLayers,
        &b_trk_nEtaLayers);
528     fChain->SetBranchAddress("trk_vx", &trk_vx, &b_trk_vx);
529     fChain->SetBranchAddress("trk_vy", &trk_vy, &b_trk_vy);
530     fChain->SetBranchAddress("trk_vz", &trk_vz, &b_trk_vz);
531     fChain->SetBranchAddress("DV_x", &DV_x, &b_DV_x);
532     fChain->SetBranchAddress("DV_y", &DV_y, &b_DV_y);
533     fChain->SetBranchAddress("DV_z", &DV_z, &b_DV_z);
534     fChain->SetBranchAddress("DV_r", &DV_r, &b_DV_r);
535     fChain->SetBranchAddress("DV_l", &DV_l, &b_DV_l);
536     fChain->SetBranchAddress("DV_m", &DV_m, &b_DV_m);
537     fChain->SetBranchAddress("DV_charge", &DV_charge, &
        b_DV_charge);
538     fChain->SetBranchAddress("DV_openAng", &DV_openAng, &
        b_DV_openAng);
539     fChain->SetBranchAddress("DV_distV", &DV_distV, &b_DV_distV)
```

```
    ;
540    fChain->SetBranchAddress("DV_muIndexLead", &DV_muIndexLead,
       &b_DV_muIndexLead);
541    fChain->SetBranchAddress("DV_muIndexSub", &DV_muIndexSub, &
       b_DV_muIndexSub);
542    Notify();
543 }
544
545 Bool_t AnalysisEdited20GeV_11_13::Notify()
546 {
547    // The Notify() function is called when a new file is opened
       . This
548    // can be either for a new TTree in a TChain or when when a
       new TTree
549    // is started when using PROOF. It is normally not necessary
        to make changes
550    // to the generated code, but the routine can be extended by
        the
551    // user if needed. The return value is currently not used.
552
553    return kTRUE;
554 }
555
556 void AnalysisEdited20GeV_11_13::Show(Long64_t entry)
557 {
558 // Print contents of entry.
559 // If entry is not specified, print current entry
560    if (!fChain) return;
561    fChain->Show(entry);
562 }
563 Int_t AnalysisEdited20GeV_11_13::Cut(Long64_t entry)
564 {
565 // This function may be called from Loop.
566 // returns  1 if entry is accepted.
567 // returns -1 otherwise.
568    return 1;
569 }
570 #endif // #ifdef AnalysisEdited20GeV_11_13_cxx
```

3. Workspace Model from RooFit: Created the Poisson Process model with Background, used for both optimistic and pessimistic approach.

```
using namespace RooFit;
using namespace RooStats;

void CountingModel(  int nobs = 127,            // number of observed events
                     double b = 127,            // number of background events
                     double sigmab = 0.3543   )    // relative uncertainty in b sigmb = 11/127 = 0.0866 //using 127+/-45, sigmab = 45/127 = 0.3543
{
  RooWorkspace w("w");

  // make Poisson model * Gaussian constraint
  w.factory("sum:nexp(s[127,0,500],b[127,0,500])");  // s[127,0,250],b[127,0,250]
  // Poisson of (n | s+b)
  w.factory("Poisson:pdf(nobs[0,500],nexp)"); //original
  w.factory("Gaussian:constraint(b0[0,500],b,sigmab[127])"); // original
  w.factory("PROD:model(pdf,constraint)");


  w.var("b0")->setVal(b);
  w.var("b0")->setConstant(true); // needed for being treated as global observables
  w.var("sigmab")->setVal(sigmab*b);


  ModelConfig mc("ModelConfig",&w);
  mc.SetPdf(*w.pdf("model"));
  mc.SetParametersOfInterest(*w.var("s"));
  mc.SetObservables(*w.var("nobs"));
  mc.SetNuisanceParameters(*w.var("b"));

  // these are needed for the hypothesis tests
  mc.SetSnapshot(*w.var("s"));
  mc.SetGlobalObservables(*w.var("b0"));

  mc.Print();
  // import model in the workspace
  w.import(mc);

  // make data set with the namber of observed events
```

```
38   RooDataSet data("data","", *w.var("nobs"));
39   w.var("nobs")->setVal(127);
40   data.add(*w.var("nobs") );
41   // import data set in workspace and save it in a file
42   w.import(data);
43
44   w.Print();
45
46   TString fileName = "CountingModel_040219.root";
47
48   // write workspace in the file (recreate file if already
       existing)
49   w.writeToFile(fileName, true);
50
51 }
```

Bibliography

[1] Particle counting statistics.

[2] Statistical analysis of data.

[3] G. Abbiendi. Search for the standard model higgs boson at lep, June 2003.

[4] S. Adler. Adventures in theoretical physics: Selected papers of stephen l. adler – commentaries, September 2005.

[5] A. Albert. How special is 3 sigma?, April 2014.

[6] F. R. F. S. H. V. M. F. M. O. S. H. S. S. T. T. P. Z. M. Alwall, J., July 2014.

[7] P. G. Astone, P. Upper limits in the case that zero events are observed: An intuitive solution to the background dependence puzzle, February 2000.

[8] F. . F. M. . F. A. . G. V. . G. P. F. . G. H. . G. C. . H. R. . H. S. . K. O. . K. S. . K. H. . L. F. . P. I. . P. I. . S. P. Barriere, J. C. ; Bauer, January 2008.

[9] C. Bini, 2014.

[10] C. Bini, 2014.

[11] C. Bini, 2014.

[12] C. Bini, 2014.

[13] J. Branson. The qed lagrangian and gauge invariance, April 2013.

[14] M. Breinig. The standard model, June 2012.

[15] P. Busch. The time–energy uncertainty relation, 2007.

[16] F. A. Bélusca-Maïto, H. On the exotic higgs decays in effective field theory. volume 79, pages 1–10, 2016.

[17] . G. P. Carithers, B. Discovery of the top quark. *Beam Line*, 25:4–16, 1995.

[18] . G. P. Carithers, B. Discovery of the top quark. volume 25, page 6, 1995.

[19] . G. P. Carithers, B. Discovery of the top quark. volume 25, page 7, 1995.

[20] . G. P. Carithers, B. Discovery of the top quark. volume 25, page 11, 1995.

[21] S. Carroll. Standard model of particle physics. In *Dark Matter, Dark Energy: The Dark Side of the Universe*, page 129. The Great Courses, 2007.

[22] CERN. Lhc experiments.

[23] A. C. CERN. History of the atlas experiment.

[24] A. Collaboration. Atlas detector.

[25] A. Collaboration. Discovery of higgs boson.

[26] A. Collaboration. Magnet system.

[27] A. Collaboration, May 2014.

[28] A. Collaboration. Search for long-lived particles in final states with displaced dimuon vertices in pp collisions at $\sqrt{s} = 13$ tev with the atlas detector, August 2018.

[29] A. Collaboration. Search for long-lived particles in final states with displaced dimuon vertices in pp collisions at $\sqrt{s} = 13$ tev with the atlas detector, August 2018.

[30] A. Collaboration. Search for long-lived particles in final states with displaced dimuon vertices in pp collisions at $\sqrt{s} = 13$ tev with the atlas detector, August 2018.

[31] W. Commons. Color charge between antiquarks.

[32] W. Commons. Color charge between quarks.

[33] E. R. G. S. J. P. K. A. L. T. L. Z. M. D. S. J. S. M. S. Z. T. B. Z. J. Curtin, D. Exotic decays of the 125 gev higgs boson, October 2017.

[34] E. R. G. S. J. P. K. A. L. T. L. Z. M. D. S. J. S. M. S. Z. T. B. Z. J. Curtin, D. Exotic decays of the 125 gev higgs boson, October 2017.

[35] E. R. G. S. J. P. K. A. L. T. L. Z. M. D. S. J. S. M. S. Z. T. B. Z. J. Curtin, D. Exotic decays of the 125 gev higgs boson, October 2017.

[36] E. R. G. S. J. P. K. A. L. T. L. Z. M. D. S. J. S. M. S. Z. T. B. Z. J. Curtin, D. Exotic decays of the 125 gev higgs boson, October 2017.

[37] E. R. G. S. S. J. Curtin, D. Illuminating dark photons with high-energy colliders, February 2015.

[38] G. Danby, J.-M. Gaillard, K. Goulianos, L. M. Lederman, N. Mistry, M. Schwartz, and J. Steinberger. Observation of high-energy neutrino reactions and the existence of two kinds of neutrinos. *Phys. Rev. Lett.*, 9:36–44, Jul 1962.

[39] S. Dawson. Introduction to electroweak symmetry breaking, January 1999.

[40] A. Experiment. Inner detector, 2009.

[41] U. S. D. o. E. P. D. G. Fermilab, Office of Science. Standard model.

[42] M. Garcia-Sciveres. The atlas pixel detector, September 2002.

[43] V. T. Gianotti F. The discovery and measurements of a higgs boson. volume 373, pages 3–12, 2015.

[44] J. Gillies. Luminosity? why don't we just say collision rate?, March 2011.

[45] M. Goossens. Calorimetry, January 1995.

[46] M. Goossens. Inner detector, January 1995.

[47] M. Goossens. Magnet system, January 1995.

[48] H. Gray and B. Mansoulié. The higgs boson: The hunt, the discovery, the study and some future perspectives, July 2018.

[49] D. Griffiths. Elementary particle dynamics. In *Introduction to Elementary Particles*, pages 55 – 62. Wiley-VCH, 2004.

[50] D. Griffiths. Elementary particle dynamics. In *Introduction to Elementary Particles*, pages 73 – 74. Wiley-VCH, 2004.

[51] D. Griffiths. Elementary particle dynamics. In *Introduction to Elementary Particles*, pages 62 – 65. Wiley-VCH, 2004.

[52] D. Griffiths. Feynman calculus. In *Introduction to Elementary Particles*, pages 190 – 191. Wiley-VCH, 2004.

[53] D. Griffiths. Historical introduction to the elementary particles. In *Introduction to Elementary Particles*, pages 11 – 13. Wiley-VCH, 2004.

[54] D. Griffiths. Quantum chromodynamics. In *Introduction to Elementary Particles*, page 280. Wiley-VCH, 2004.

[55] F. Huegging, August 2005.

[56] P. Iengo, June 2011.

[57] L. Jeanty, August 2007.

[58] D. Kaiser. Physics and feynman's diagrams. *American Scientist*, 93:156 – 165, March - April 2005.

[59] H. Kate. Superconducting magnet system for the atlas detector at cern. volume 9 of *2*, pages 841–846, 1999.

[60] T. Kibble. Glashow-weinberg-salam model: An example of electroweak symmetry breaking, February 2015.

[61] V. R. Kidonakis, N., August 2003.

[62] U. N. A. C. S. N. T. G. Y. P. . . . S. J. Kodama, K. Observation of tau neutrino interactions. *Phys. Letters B*, 504:218–224, 2001.

[63] D. Kwon. Where does mass come from?, May 2016.

[64] H. Leutwyler. On the history of the strong interaction, November 2012.

[65] L. Lista. Practical statistics for particle physicists, July 2017.

[66] G. C. J. D. M. Robinson, K. Bland. A simple introduction to particle physics, October 2008.

[67] B. Martin and G. Shaw. Gauge theories. In *Particle Physics*, page 374. Wiley, 2008.

[68] B. Martin and G. Shaw. Leptons and the weak interaction. In *Particle Physics*, pages 28 – 29. Wiley, 2008.

[69] B. Martin and G. Shaw. Leptons and the weak interaction. In *Particle Physics*, pages 32 – 35. Wiley, 2008.

[70] B. Martin and G. Shaw. Qcd, jets, and gluons. In *Particle Physics*, page 181. Wiley, 2008.

[71] B. Martin and G. Shaw. Quark model. In *Particle Physics*, page 163. Wiley, 2008.

[72] B. Martin and G. Shaw. Quarks and hadrons. In *Particle Physics*, pages 51 – 56. Wiley, 2008.

[73] B. Martin and G. Shaw. Some basic concepts. In *Particle Physics*, pages 1–2, 19. Wiley, 2008.

[74] A. R. Martínez. The run-2 atlas trigger system. volume 762, pages 1–9, 2016.

[75] B. Mindur, March 2016.

[76] A. T. C. Mitsou, V. A., November 2003.

[77] J. Morris. Hep analysis. Technical report, Queen Mary University of London, 2012.

[78] R. Nave. Hyperphysics, bosons.

[79] R. Nave. Hyperphysics, fermions.

[80] R. Nave. Hyperphysics, the color force.

[81] R. Nave. Hyperphysics, weak force.

[82] A. C. Pastore, F. Tthe atlas trigger system: Past, present and future. volume 273-275, pages 1065–1071, 2016.

[83] D. H. Perkins. Interaction and fields. In *Introduction to High Energy Physics*, pages 42 – 43. Cambridge University Press, 2012.

[84] M. L. Perl, G. S. Abrams, A. M. Boyarski, M. Breidenbach, D. D. Briggs, F. Bulos, W. Chinowsky, J. T. Dakin, G. J. Feldman, C. E. Friedberg, D. Fryberger, G. Goldhaber, G. Hanson, F. B. Heile, B. Jean-Marie, J. A. Kadyk, R. R. Larsen, A. M. Litke, D. Lüke, B. A. Lulu, V. Lüth, D. Lyon, C. C. Morehouse, J. M. Paterson, F. M. Pierre, T. P. Pun, P. A. Rapidis, B. Richter, B. Sadoulet, R. F. Schwitters, W. Tanenbaum, G. H. Trilling, F. Vannucci, J. S. Whitaker, F. C. Winkelmann, and J. E. Wiss. Evidence for anomalous lepton production in $e^+ - e^-$ annihilation. *Phys. Rev. Lett.*, 35:1489–1492, Dec 1975.

[85] L. Pontecorvo. The atlas muon spectrometer. volume 34, pages 117–128, 2004.

[86] F. Porter, December 2001.

[87] P. R. Poudel. Quarks and their discovery. *Himalayan Physics*, 1:65, 200.

[88] P. Puzo. Atlas calorimetry. volume 494, pages 340–345, year =.

[89] G. Rajasekaran. Fermi and the theory of weak interactions. volume 19, pages 2–4, 2014.

[90] G. Rajasekaran. Fermi and the theory of weak interactions. volume 19, pages 10 – 18, 2014.

[91] J. Snuverink. *The ATLAS Muon Spectrometer: Commissioning and Tracking*. PhD thesis, Nikhef, October 2009.

[92] C. Stubbs. Early unifications for electromagnetism, 2010.

[93] P. Tanedo. Why do we expect a higgs boson? part i: Electroweak symmetry breaking, 2011.

[94] L. Taylor. Higgs boson, November 2011.

[95] J. J. M. F. Thomson. Cathode Rays. *The London, Edinburgh, and Dublin Philosophical Magazine and Journal of Science*, 44(293 - 316):1, 1897.

[96] . A. S. C. Turala, M. The atlas semiconductor tracker. volume 466, pages 243–254, 2001.

[97] J. D. Wells. The theoretical physics ecosystem behind the discovery of the higgs boson, September 2016.

[98] F. L. Wilson. Fermi's theory of beta decay. volume 36, page 1150, 1968.

[99] J. Woithe, G. Wiener, and F. Van der Veken. Let's have a coffee with the Standard Model of particle physics! *Physics Education*, 52(3):1, 2017.

[100] X. Xin. Glashow-weinberg-salam model: An example of electroweak symmetry breaking, December 2007.

[101] M. Zur Nedden, October 2011.